Asteroseismology

Dominic M. Bowman[a,b] and Lisa Bugnet[c]
[a]School of Mathematics, Statistics and Physics, Newcastle University, Newcastle upon Tyne, NE1 7RU, UK
dominic.bowman@newcastle.ac.uk
[b]Institute of Astronomy, KU Leuven, Celestijnenlaan 200D, 3001 Leuven, Belgium
[c]Institute of Science and Technology Austria, (ISTA), Am Campus 1, Klosterneuburg, Austria

© 20xx Elsevier Ltd. All rights reserved.
Chapter Article tagline: update of previous edition,, reprint..

Abstract

Asteroseismology is the study of the interior physics of stars using their pulsations. It is applicable to stars across the Hertzsprung–Russell (HR) diagram and a powerful technique to directly constrain interior rotation, chemical mixing, and magnetism. This is because a star's self-excited pulsation modes are sensitive to its structure. Asteroseismology generally requires long-duration and high-precision time series data and the method of forward asteroseismic modelling. This is the statistical comparison of observed pulsation mode frequencies to theoretically predicted pulsation frequencies calculated from a grid models, and provides precise masses and ages for calibrating various transport phenomena. In this introduction to asteroseismology, we provide an overview of its principles, and the typical data sets and methodologies used to constrain stellar interiors. Finally, we present a few key highlights of asteroseismic results from across the HR diagram, and conclude with ongoing challenges and future prospects for this ever-expanding field within stellar astrophysics.

Keywords: Asteroseismology (73); Stellar oscillations (1617); Stellar structures (1631); Stellar evolution (1599); Stellar rotation (1629); Stellar magnetic fields (1610)

Learning Objectives

1. The basic principles and fundamentals of asteroseismology.
2. The common data sets and analysis methods used for analysing stellar pulsations.
3. The definitions of different types of pulsating stars within the HR diagram.
4. The diversity in pulsation frequencies and amplitudes across different types of pulsators.
5. Key examples of important results from asteroseismology in recent decades.
6. The remaining major uncertainties in stellar structure and evolution theory yet to be fully solved.

Glossary

Eddington limit: When radiative acceleration acting outwards is balanced by gravity acting inwards, and defines the maximum ratio of L/M for a star in hydrostatic equilibrium.
Gravity mode: Type of pulsation mode with a standing wave that has buoyancy as the restoring force.
Hertzsprung–Russell (HR) diagram: Diagnostic diagram that plots stellar effective temperatures versus their luminosities, and reveals the evolutionary stages for an ensemble of stars.
Hydrostatic equilibrium: The balance of gravity acting inwards and gas pressure from nuclear fusion acting outwards.
Iterative prewhitening: Methodology to identify significant pulsation mode frequencies from a time series (e.g. light curve), which utilises Fourier analysis to identify significant pulsation mode frequencies, and then least-squares regression to optimise significant frequencies using a sinusoid model. This model is subtracted from the time series to produce a residual time series and residual frequency spectrum. The process repeats in an iterative fashion until all pulsation mode frequencies have been identified.
Kraft break: A divider in mass on the main sequence at approximately 1.5 $M_{\odot}$ that separates fast-rotating higher mass stars and slow-rotating low-mass stars, which corresponds to a spectral type of about F5 V.
Main sequence: The longest part of a star's total lifespan, during which it undergoes hydrogen burning through nuclear fusion in its core.
Mixed mode: Type of pulsation mode with a standing wave that has the properties of gravity mode in the deep interior and the properties of a pressure mode in the envelope.
Pressure mode: Type of pulsation mode with a standing (sound; acoustic) wave that has the pressure gradient as the restoring force.
Population II **stars**: Old and metal-poor stars often found in the bulges and halos of galaxies that were born in a previous generation of star formation relative to the younger and metal-rich Population I stars born relatively recently in the disks of spiral galaxies.
Red Giant Branch (RGB) star: An evolved low-mass star that is characterised by being more luminous and redder in colour compared to the Sun, and in the hydrogen-shell burning phase of stellar evolution.
Schwarzschild criterion: Definition for whether a region's dominant energy transport mechanism is convection, with convection occurring if either (i) the radiative temperature gradient is steep enough; or (ii) the adiabatic temperature gradient is shallow enough.

Spherical harmonics: Solutions for oscillations on the surface of a sphere and includes three quantum numbers: the radial order (n) which defines the number of nodes in the radial direction; the angular degree (ℓ) which defines the number of surface nodal lines; and the azimuthal order (m) which defines the number of surface nodal lines that are lines of longitude, such that $|m| \leq \ell$.
Strange mode: Type of non-linear radial pulsation-like instability caused by the strong enhancements in the non-adiabatic partial ionization zones in stars near the Eddington limit (e.g. very massive stars).
Stochastic low-frequency (SLF) variability: A non-periodic form of variability detected to be seemingly ubiquitous in the light curves of massive stars, likely to be caused by gravity waves that are stochastically excited from interior convection zones.
Solar-like oscillator (SLO): A group of pulsating stars with stochastically excited pulsations driven by turbulent envelope convection, such that they have the same pulsation excitation mechanism to the Sun. This group predominantly includes solar-type stars and red giant branch (RGB) stars.

Nomenclature and Common Units

d^{-1}	cycles-per-day, frequency unit used for stellar pulsation frequencies
$M_\odot$	Solar mass (1.99×10^{30} kg)
mmag	milli-magnitudes, flux unit used to measure the brightness variations of a star
μHz	micro-Hertz, frequency unit used for stellar pulsation frequencies
$R_\odot$	Solar radius (6.96×10^8 m)
ppm	parts-per-million, flux unit used to measure the brightness variations of a star

1 Introduction

In astrophysics one of the most fundamental parameters of a star is its mass. Stars are generally divided into three main groups based on their birth masses: (i) low-mass stars with masses of $M \lesssim 1.3$ $M_\odot$; (ii) intermediate-mass stars with masses of $1.3 \lesssim M \lesssim 8$ $M_\odot$; and (iii) massive stars with masses of $M \gtrsim 8$ $M_\odot$. These definitions of mass regimes are in part motivated by the fact that a star's hydrostatic equilibrium structure differs significantly across these groups during the longest part of their lifetimes, the hydrogen-core burning main-sequence phase. For example, the distinction between low-mass and intermediate-mass stars is motivated by intermediate-mass stars having convective hydrogen-burning cores and radiative envelopes. Whereas low-mass main-sequence stars, like our Sun, have radiative hydrogen-burning cores and convective envelopes (Kippenhahn et al., 2012). Schematics of the differences in structure of three example stars are shown in Fig. 1. Another important aspect of the three mass-regime definitions is the difference in their evolutionary end products. Massive stars are progenitors of core-collapse supernovae and gamma ray bursts, and leave behind neutron stars and black holes as compact remnants at the ends of their lives (Langer, 2012). On the other hand, intermediate- and low-mass stars are progenitors of planetary nebulae and white dwarfs (Kippenhahn et al., 2012).

During the longest-lived phase of stellar evolution – the main sequence – a star is referred to as a dwarf star since it is relatively small whilst it depletes its supply of hydrogen fuel. In order to maintain hydrostatic equilibrium, the increase in mean molecular weight through nuclear fusion in the hydrogen-burning core results in a gradual increase in radius. However, once the hydrogen is depleted entirely, a star has entered the post-main sequence in which its envelope grows to a much larger size in a relatively short amount of time. Post-main sequence stars are referred to as sub-giants and giants in the low- and intermediate-mass regimes and supergiants in the massive-star regime. Dependent on its mass, there are a number of epochs of nuclear burning phases of chemical elements heavier than hydrogen until it is no longer energetically favourable to continue nuclear fusion. Also, different layers within the star can change between having radiation or convection as the dominant energy transport mechanism following the Schwarzschild criterion (Kippenhahn et al., 2012). This is important since different types of oscillations (i.e. pulsations) are more or less sensitive to radiative and convection zones within a star.

Similar to how the frequency of sound waves generated by a person's vibrating vocal cords depend on the density, temperature and chemical composition of the air they are breathing, the natural resonant frequencies of pulsations in a star depend on its mass, radius, age and chemical composition. Therefore, by measuring the frequencies of a star's pulsations, one is able to constrain its and its mass, radius and age, but also its interior properties, such as which layers are undergoing nuclear burning and their dominant energy transport mechanism. This defines the field of asteroseismology as the study of stellar pulsations for the purpose of improving our understanding of stellar structure and evolution theory within astrophysics. Asteroseismology has rapidly grown to become a mature and advanced field in recent decades, primarily to its success in providing extremely high-precision constraints on stellar properties compared to more traditional methods in astrophysics. Aerts et al. (2010) provides a complete monograph on asteroseismology aimed at postgraduate students and beyond. Whereas, Aerts (2021) and Kurtz (2022) provide extensive and recent reviews of how the theoretical and observational aspects of asteroseismology have progressed in the last two decades, respectively.

The goal of this chapter on asteroseismology in the Encyclopedia of Astrophysics is to provide a modern entry-point for early-career researchers, such as undergraduate and postgraduate students, into the expanding field of asteroseismology. Here we summarise the basic principles of asteroseismology in Section 2, its common data sets and methods in Section 3, and highlight some key modern results of asteroseismology in the literature from the last two decades in Section 4. We conclude and provide a summary of the ongoing challenges and future opportunities in Section 5.

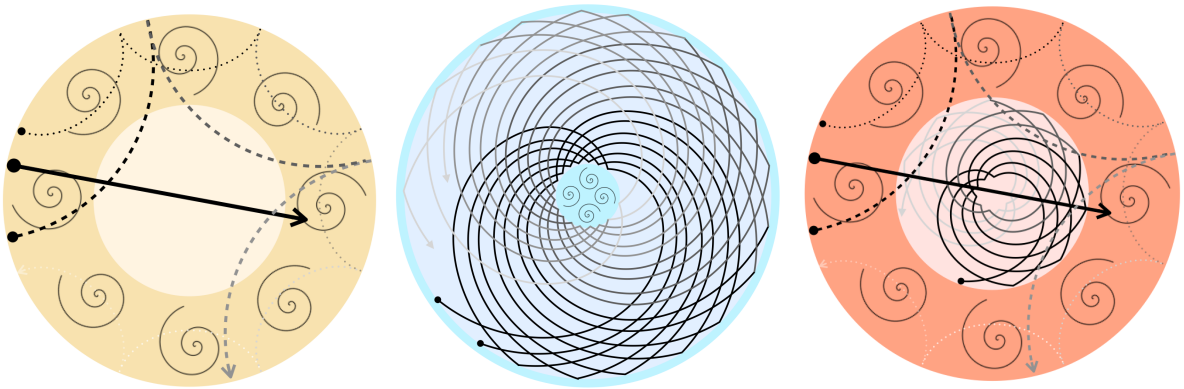

Fig. 1 Schematics of the different structures of example pulsating stars. Left Panel: Low-mass main-sequence star like the Sun, with the convective envelope indicated by darker yellow area marked by vortexes, and the radiative interior shown in pale yellow. Each ray-tracing path represents an individual pulsation mode that starts at a black circle: The continuous arrow indicates a radial pulsation mode, the dashed arrow indicates a quadrupolar mode, and the dotted line indicates the propagation of a high-radial order high-angular degree mode constrained near the surface. Middle Panel: A more massive star, such as a slowly pulsating B-type (SPB) star (see Fig. 2), which has a convective core during the main sequence and hosts gravity modes in the radiative envelope. Right Panel: Red giant branch (RGB) star hosting mixed gravito-acoustic modes that probe its convective envelope and radiative interior.

2 Stellar pulsations

Asteroseismology is a powerful method for constraining the interior physical conditions and transport processes of stars – see monograph by Aerts et al. (2010). At its heart is the principle that the self-excited resonant pulsation modes of a star represent small perturbations to its hydrostatic equilibrium structure. Since stellar pulsation modes directly probe a star's structure, it follows that the fundamental data of asteroseismology are the Eigenfrequencies of a star, which correspond to pulsation modes (i.e. standing waves) each with a unique spherical harmonic geometry. For non-rotating and non-magnetic stars, the wave functions of a star's pulsations are separable into radial and angular components, with the radial component characterised by a radial order (n) defining the number of interior shells acting as nodes, and the angular component characterised by an angular degree (ℓ), which defines the number of nodal lines on the surface, and an azimuthal order (m), which is how many surface nodal lines are lines of longitude such that $|m| \leq \ell$. Thus, it is an important goal of asteroseismology to identify the frequencies of pulsations in terms of spherical harmonic geometry, and ultimately compare them to theoretical models to constrain a star's physics using a robust statistical comparison methodology — see review by Aerts (2021).

Schematic examples of different pulsation cavities for different types of standing waves for a low-mass main-sequence star like the Sun, a main-sequence more massive star such as a slowly pulsating B-type (SPB) star, and a red giant branch (RGB) star are shown schematically in Fig. 1, which are set by the physics of their interiors. Consequently, different stellar structures provide the necessary conditions to excite different types of pulsation modes, such that pulsations are expected across the Hertzsprung–Russell (HR) diagram. An asteroseismic HR diagram in which the main types of pulsators are labelled is shown in Fig. 2. The different types of pulsation modes responsible for the plethora of pulsating stars across the HR diagram are explained in the following subsections.

2.1 Pressure modes

Pressure modes are standing sounds waves for which the pressure gradient acts as the dominant restoring force, and they can have radial ($\ell = 0$) or non-radial (i.e. $\ell \geq 1$) spherical harmonic geometries. For radial pressure modes, since there is no angular dependence, it is the entire radius of a star that acts as the pulsation cavity. Whereas non-radial pressure modes can only penetrate to a certain depth beneath the stellar surface, which is determined by the local adiabatic sound speed, $c_{\rm s}$, defined as:

$$c_{\rm s} = s\sqrt{\gamma\frac{P}{\rho}}, \tag{1}$$

where γ is the adiabatic index, P is the pressure, and ρ is the density of the gas. The pulsation cavity of a pressure mode is related to the requirement of it having a frequency higher than the Lamb frequency, S_ℓ, which is defined as:

$$S_\ell = \frac{\ell(\ell+1)\,c_{\rm s}^2}{r^2}. \tag{2}$$

Rearranging Eqn. (2) for radius, r, defines the so-called 'turning radius' of a non-radial pressure mode. This is the deepest radial coordinate a non-radial pressure mode reaches if excited at the stellar surface. Thus, pressure modes with higher values of ℓ have shallower pulsation cavities since the turning radius is proportional to $\sqrt{\ell(\ell+1)}$, which means that higher-ℓ pressure modes are more sensitive to the near-surface layers within a star as shown in the schematic in the left panel of Fig. 1.

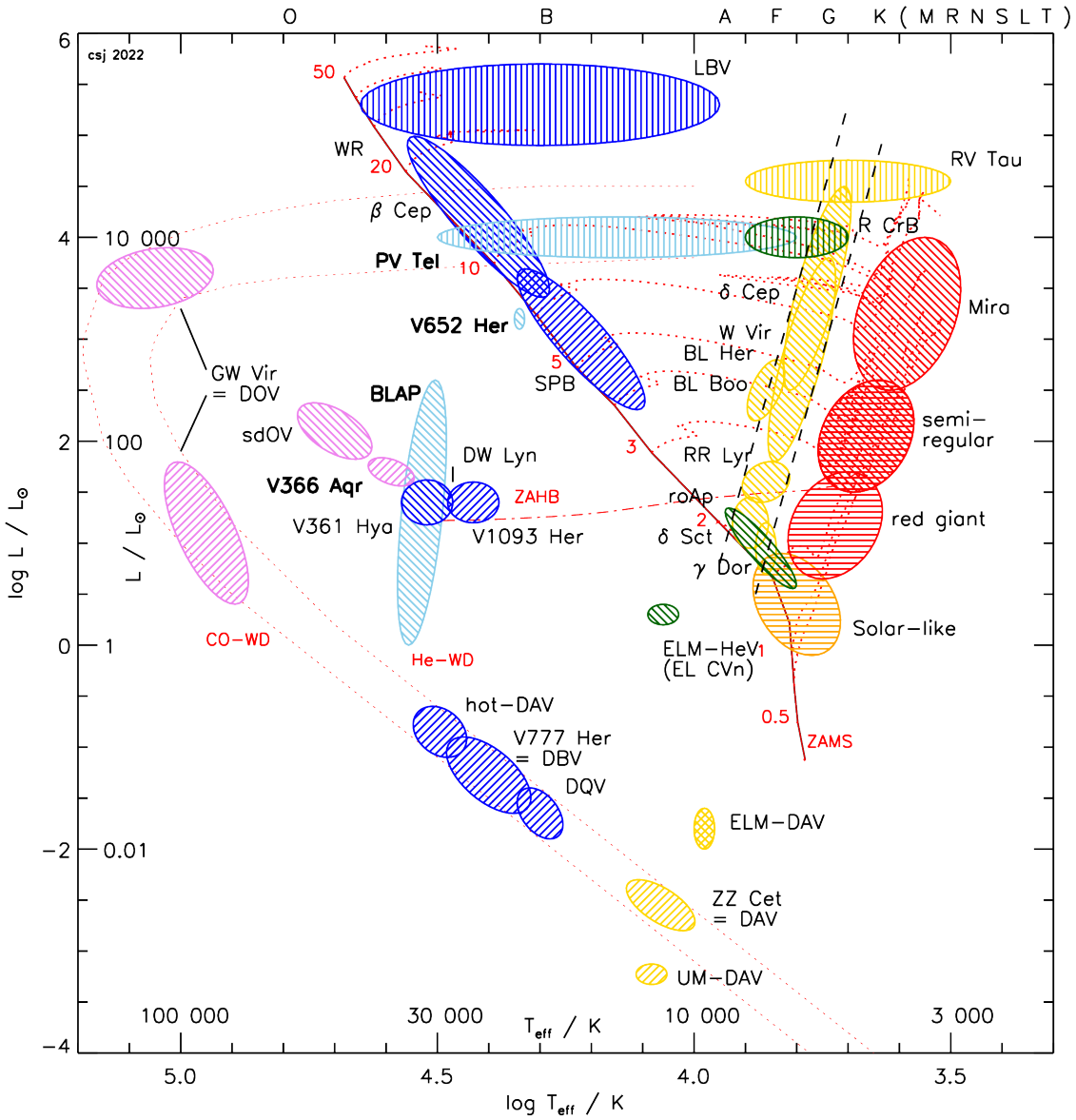

Fig. 2 Hertzsprung–Russell (HR) diagram of different pulsator classes, courtesy of C. S. Jeffery and based on figure 1 from Kurtz (2022). The hatching of a region denotes the dominant types of modes for the stars it contains: pressure (p) modes (\\\), gravity (g) modes (///), stochastically driven pulsators (≡), and strange modes (|||). Evolutionary tracks of various masses are shown as dotted lines in units of $M_\odot$, with the zero-age main-sequence (ZAMS) line shown as a solid line. The classical instability strip containing the Cepheid variables at high luminosities and δ Scuti stars at the intersection with the ZAMS line is delimited by two dashed lines. The zero-age helium-burning (ZAHB) is shown as a dash-dot line, as well as the white dwarf cooling track.

For pressure modes with relatively high-radial orders such that $n >> \ell$, with typical values being $n \in \{5, ..., 15\}$ and $\ell \in \{0, 1, 2\}$, the frequencies follow an asymptotic approximation such that pressure modes of consecutive radial order (n) with the same angular degree (ℓ) and azimuthal order (m) are equally spaced in frequency. The frequency difference within this regular 'comb' of frequencies defines the large frequency separation:

$$\Delta\nu = \left(2\int_0^R \frac{\mathrm{d}r}{c_\mathrm{s}}\right)^{-1}, \tag{3}$$

which is a measure of the mean density of a star since it is inverse of the sound crossing time.

Another useful observable to determine when analysing stars with high-radial order pressure modes is the frequency of maximum power, often denoted as ν_max. Although there is some uncertainty as to how specific radial-order pressure modes are excited by turbulent convection

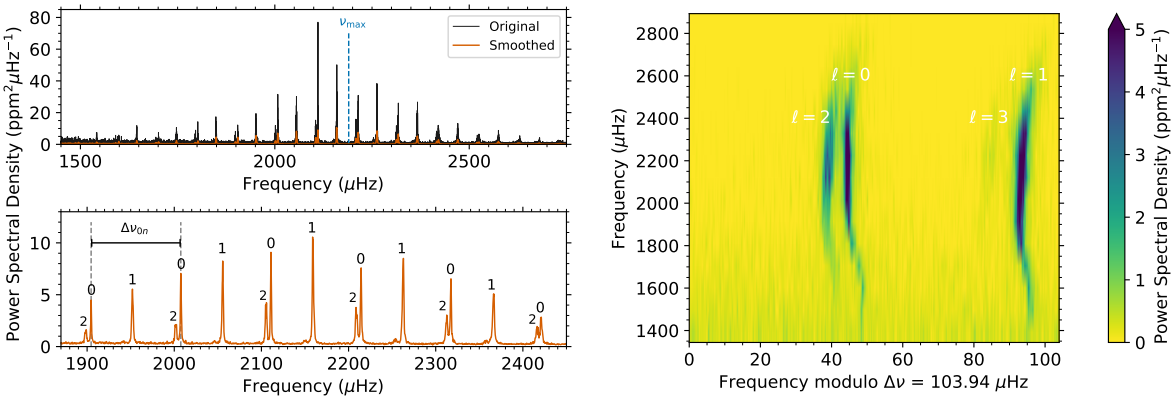

Fig. 3 Left Panels: Power spectral density (PSD) spectrum of the solar "twin" star 16 Cyg A calculated from a light curve assembled by the *Kepler* mission. The top-left panel shows the frequency regime containing all the significant pressure modes. The bottom-left panel shows a zoom-in of the smoothed PSD spectrum with the angular degree, ℓ, of individual pulsation modes labelled, as well as the large frequency separation, $\Delta\nu = 103.94$ μHz, and frequency of maximum power, $\nu_{\rm max}$, at a frequency of about 2200 μHz. Right panel: Echelle diagram of 16 Cyg A with the dominant $\ell = 0, 1, 2$ and barely visible $\ell = 3$ ridges of pulsation modes separated by $\Delta\nu$.

in a star like the Sun, a roughly Gaussian envelope of energy is typically injected into a specific frequency regime for solar-like oscillators (SLOs), which includes solar-type stars and RGB stars (Chaplin and Miglio, 2013). The power excess thus can be approximated by a Gaussian with a centroid corresponding to $\nu_{\rm max}$. As stars evolve, such as when a star ascends the RGB whilst hydrogen-shell burning, the value of $\nu_{\rm max}$ moves to lower frequencies, driven by a star's increasing radius. It is expected from theory and seen in observations that $\nu_{\rm max}$ follows the relationship: $\nu_{\rm max} \propto \nu_{\rm ac} \propto g T_{\rm eff}^{-1/2}$, where $T_{\rm eff}$ is the effective temperature of the star, and $\nu_{\rm ac}$ is the acoustic cut-off frequency, which is the highest frequency pressure mode that can be supported within a star given its mass and radius (Hekker, 2020). Given this proportionality relationship and by measuring the Sun's $\nu_{\rm max}$ value from the frequency spectrum of its light curve, one can derive:

$$\nu_{\rm max} = \frac{M/M_\odot}{(R/R_\odot)^2 \sqrt{T_{\rm eff}/T_{\rm eff,\odot}}} \nu_{\rm max,\odot} \,, \tag{4}$$

where $\nu_{\rm max,\odot} = 3050$ μHz and $T_{\rm eff,\odot} = 5777$ K are the solar values.

The regular pattern of high-radial order pressure modes equally spaced in frequency and centered on a particular frequency results in measurable values of $\Delta\nu$ and $\nu_{\rm max}$, respectively. These are most readily apparent in the frequency spectra of SLOs including the Sun and RGB stars. An example of the frequency spectrum of the SLO star 16 Cyg A is shown in Fig. 3, in which the individual pulsation modes are labelled, as well as the observables $\Delta\nu$ and $\nu_{\rm max}$. The relationship in Eqn. (4) demonstrates that younger stars have higher values of $\nu_{\rm max}$ to older stars of the same mass. This means that 16 Cyg A is an older star compared to the Sun given it has a comparable mass of 1.08 ± 0.02 M$_\odot$ (Chaplin and Miglio, 2013).

For pulsating stars with regular series of pressure modes in their frequency spectra, such as solar-type stars and RGB stars, common methods to identify $\Delta\nu$, and hence obtain the spherical harmonic geometry mode identification, are to directly fit the regular pattern in the frequency spectrum, or use a technique known as an Echelle diagram (Chaplin and Miglio, 2013; Hekker, 2020). The former can be fairly computational expensive, whereas the latter can efficiently be used in either a manual or semi-automatic approach. An Echelle diagram is a frequency spectrum that has been divided into equal sections with a width that represents the distance between the rungs of a 'ladder'. In so doing, for pressure mode pulsations that have the asymptotic property of being equally spaced in frequency, the spacing between a comb of frequencies can be derived and used to determine $\Delta\nu$. Since the definition of $\Delta\nu$ is the frequency spacing of pressure modes of consecutive radial order but the same angular degree and azimuthal order, the identification of $\Delta\nu$ means ℓ and m values of pulsation modes can be assigned. An example of an Echelle diagram for the SLO star 16 Cyg A is shown in Fig. 3, in which the dominant ridges corresponding to the $\ell = 0, 1, 2$ and barely visible $\ell = 3$ series of equally-spaced pressure modes are labelled. Strictly speaking, Eqn. (3) dictates that asymptotic pressure modes are exactly equally spaced in frequency. As can be seen in Fig. 3, however, this is not the case, and a small curvature in the Echelle ridges of pulsation modes can be seen. This discrepancies are caused by the physical conditions and processes within a star's envelope, such as the glitches in temperature and/or chemical composition profiles near partial ionisation zones (Chaplin and Miglio, 2013). These are details of the structure of a star that are not captured in Eqn. (3).

2.2 Gravity modes

Gravity modes are standing waves with buoyancy (i.e., gravity) as their dominant restoring force, and as such they have lower frequencies compared to their pressure-mode counterparts. Gravity modes can only have non-radial ($\ell \geq 1$) spherical harmonic geometry and are defined

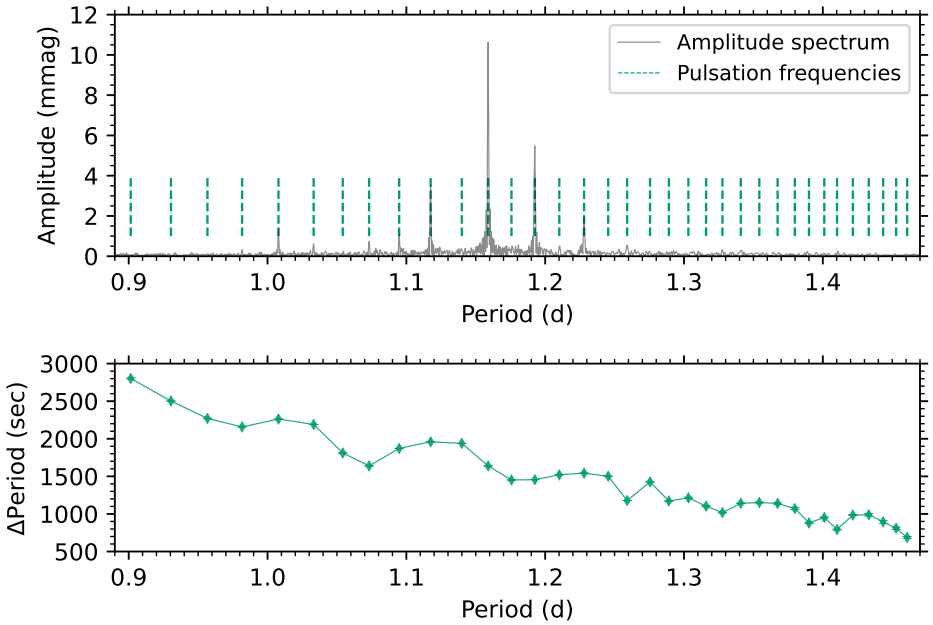

Fig. 4 Top Panel: Amplitude spectrum as a function of period for the SPB star KIC 7760680 (Bowman and Michielsen, 2021), in which the significant gravity-mode pulsation frequencies identified using iterative pre-whitening by are marked. Bottom Panel: corresponding gravity-period spacing pattern of the significant gravity-mode pulsation frequencies. Note that error bars are plotted, but are generally smaller than the symbol size owing to long duration and extremely high-photometric precision of the *Kepler* space mission.

by having frequencies lower than the Brunt-Väisälä frequency, N, (also known as the buoyancy frequency) defined as:

$$N^2 = g\left(\frac{1}{\gamma P}\frac{\mathrm{d}P}{\mathrm{d}r} - \frac{1}{\rho}\frac{\mathrm{d}\rho}{\mathrm{d}r}\right). \tag{5}$$

Analogous to the large frequency separation ($\Delta\nu$) for pressure modes, high-radial order gravity modes in the asymptotic regime are equally spaced in period and exhibit a characteristic period, Π_0, which is defined as:

$$\Pi_0 = 2\pi^2\left(\int_{r_1}^{r_2} N(r)\frac{\mathrm{d}r}{r}\right)^{-1}, \tag{6}$$

where the limits of the integral, r_1 and r_2, define the inner and outer radial coordinates of the gravity-mode pulsation cavity. The asymptotic period, Π_0, can also be calculated from fitting the periods of individual gravity modes, $P_{n\ell}$, via:

$$P_{n\ell} = \frac{\Pi_0}{\sqrt{\ell(\ell+1)}}(|n| + \alpha), \tag{7}$$

where α is phase term independent of a gravity mode's angular degree.

Given the asymptotic property of high-radial order gravity modes being equally spaced in period, a common diagnostic to analyse them and perform mode identification is to construct a gravity-mode period spacing diagram. This showcases the period differences of consecutive radial order (n) gravity modes of the same angular degree (ℓ) and azimuthal order (m) plotted as a function of pulsation mode period. An example of a gravity-mode period spacing pattern is shown in Fig. 4 for the slowly-pulsating B-type (SPB) star KIC 7760680. This star currently holds the record for the longest period spacing pattern in an SPB star, and thus has excellent precision on its interior physical processes (e.g. Bowman and Michielsen 2021). The definition of a gravity-mode period spacing pattern also means the hurdle of mode identification for pulsating stars with gravity modes is greatly alleviated.

Once constructed, there are two main features of gravity-mode period spacing diagrams exploited by asteroseismology. First is that rotation induces a gradient in the pattern, as shown in the example of KIC 7760680 in Fig. 4, such that faster rotating stars have larger 'tilts' in their patterns. Second, perturbations to a constant period spacing in addition to rotation come in the form of dips and 'wiggles' caused by trapping of pulsation modes within zones containing chemical composition gradients. This is expected because of the chemical composition term in Eqns. (5) and (6), and can also be seen in example of KIC 7760680 in Fig. 4. This means that the periods of individual gravity modes and the dips in gravity-mode period spacing patterns provide direct insight of the age of a star since the size of chemical gradient zones change during a star's evolution. However, there is a degeneracy among the mass, age and amount of chemical mixing when determining the morphology of the dips in a gravity-mode period-spacing pattern. For example, older and more-massive stars with a large

amount of interior mixing can have similar gravity-mode period spacing patterns to younger less-massive stars with smaller amounts of interior mixing, which is then further compounded by an unknown rotation rate (Bowman, 2020).

It is worth noting, that gravity modes are more commonly exploited in intermediate- and massive stars since gravity modes are evanescent in a convection zone. The amplitudes of gravity modes decay too quickly before reaching the surfaces of low-mass stars because of their thick convective envelopes. Whereas gravity modes have detectable surface amplitudes in main-sequence high- and intermediate-mass stars because of their radiative envelopes. Gravity modes are most sensitive to the region just outside of the hydrogen-burning convective core in such stars, which shrinks in size throughout the main sequence. This is because the Brunt-Väsäilä frequency, N, is zero inside a convective core, and the chemical composition gradient zone just outside a convective core in addition to the energy transport mechanism at the convective-radiative interface causes a large spike in N. The N-spike leads to trapping of the gravity modes, meaning they are most sensitive to the boundary layer between the convective core and radiative envelope. This is why the dips in gravity-mode period spacing patterns allow direct insight of the age of a star and the amount of mixing at this boundary.

2.3 Mixed modes

For main-sequence stars, the pulsation cavities of pressure and gravity modes are generally well separated within a star's interior owing to a large difference in the buoyancy and Lamb frequencies. However, as stars age these cavities expand and span larger fractions of a star's radius. Eventually they become close enough to one another to allow mixed modes, which are standing wave pulsations with gravity-mode characteristics whilst in the deep interior and pressure-mode characteristics near the surface. Moreover, the frequencies of pressure and gravity modes in evolved stars are close enough to each other such that individual pulsation modes can undergo a from of mode interaction called avoided crossings, in which individual pulsation modes 'bump' each other at specific epochs of stellar evolution (Aerts et al., 2010).

Mixed modes are only expected for post-main sequence low- and intermediate-mass stars, such as RGB stars. Asteroseismology using mixed modes has been hugely successful for evolved low- and intermediate-mass stars. Specifically, the period-spacing patterns of mixed modes has been used to distinguish the shell-hydrogen and core-helium burning phases of stellar evolution (Bedding et al., 2011). Also, since mixed modes probe the full radius of the star, they can be used to probe the radial rotation profile (Beck et al., 2012). Ensemble asteroseismic studies have revealed that tens of thousands of pulsating RGB stars have only small amounts of radial differential rotation (Aerts, 2021). Additionally precise masses and radii have been measured through the application of the asteroseismic scaling relations (Chaplin and Miglio, 2013). At the other end of the HR diagram, mixed modes are expected during the main sequence phase of massive star evolution, and can be exploited to provide precise constraints on the masses and ages of massive stars (e.g. Burssens et al. 2023).

2.4 Pulsation excitation mechanisms

There are two main pulsation excitation mechanisms. The first is the stochastic solar-like mechanism that operates within large convective envelopes and defines the pulsator group of SLOs (Chaplin and Miglio, 2013). The turbulent convection in the envelopes of main-sequence low-mass stars and evolved intermediate- and low-mass stars continuously drives and damps the resonant Eigenfrequencies of a star. An analogy would be taking a gong or bell into the middle of a sandstorm and hearing it hum atonally because of the repeated impacts of many random sand grains. As discussed in Section 2.1, the stochastic pulsation excitation mechanism in low-mass stars typically excites moderate-to-high radial order pressure modes within a certain frequency range, which is centered a frequency of maximum power: $\nu_{\rm max}$ (Chaplin and Miglio, 2013). Owing to the stochastic nature of this excitation mechanism, such pulsation modes appear as Lorentzian peaks in a frequency spectrum because they have finite mode lifetime. This is illustrated for the SLO star 16 Cyg in Fig. 3.

The second main pulsation excitation mechanism is an opacity heat-engine mechanism in which mechanical work is converted from heat energy, like a piston in an engine. Within the radiative envelopes of massive and intermediate-mass stars, there are thin partial ionisation zones at specific temperatures for hydrogen, helium and metals such as iron and nickel, in which the medium exists in transition phase from being fully ionised deeper within the star and neutral closer to the surface. The presence of partially ionised metals within the hydrogen-rich envelope creates a local source of opacity. This increased opacity blocks the outward flow of radiation, which heats the zone and causes it to expand. After expanding, the radiation is able to flow through the layer unimpeded, which means the source of heating has been removed so the layer cools down and contracts once again. The contraction leads to re-creating the (partial) ionisation zone, thus re-creates the source of opacity once again. This periodic expansion-contraction cycle allows heat from the star to be converted into mechanical work and excite pulsations (Pamyatnykh, 1999).

3 Data and methods of asteroseismology

In this section, we provide an overview of the practical data analysis steps in asteroseismology. There are usually a few fundamental steps in asteroseismology: (i) the observational component in which pulsation mode frequencies are extracted, optimised and identified; (ii) analysis of the frequencies to perform mode identification and inference of rotation or magnetic fields; and (iii) the modelling component in which the pulsation frequencies are exploited through a statistical comparison to numerical models of stellar structure and evolution to constrain their physical parameters. This full proceedure is commonly referred to as forward asteroseismic modelling (Bowman, 2020; Aerts, 2021).

3.1 Observations of pulsation frequencies

Prior to mode identification of pulsation mode frequencies in terms of spherical harmonic geometry, one must first extract the frequencies themselves. This is achieved by assembling time-series data of a star's observable surface properties. Such time series data can be: (i)

spectroscopic such that quantification of periodic changes in the profiles of spectral lines, or (ii) time-series photometry, with the periodic variability of a star's integrated brightness as a function of time often called a light curve. Asteroseismology requires time series data to have a short cadence (i.e. short integration time) to avoid smearing of the pulsation signal and ensuring it is well sampled. Time series should also be long in duration such that the frequency resolution, which is proportional to the inverse of the length of the data set, is sufficient to distinguish closely-spaced pulsation mode frequencies.

To extract pulsation mode frequencies from a time series, it is common practice to employ Fourier analysis. Time series data are discrete and finite, so a frequency spectrum is calculated numerically using, for example, the discrete Fourier transform for unevenly sampled time series (Kurtz, 1985) or a Lomb-Scargle periodogram (Scargle, 1982). The frequency spectrum is generally calculated up to the Nyquist frequency, $\nu_{\rm Nyquist}$, which is defined as:

$$\nu_{\rm Nyquist} = \frac{1}{2\Delta T}, \tag{8}$$

where ΔT is the length of the time series. The Nyquist frequency, $\nu_{\rm Nyquist}$, defines the upper frequency limit that is not under sampled, such that variability with a period of $1/\nu_{\rm Nyquist}$ is sampled with two epochs per period. Once the frequency spectrum has been calculated, peaks are denoted as statistically significant and represent pulsation mode frequencies based on satisfying a significance criterion. For example, this can be a false alarm probability (FAP) or a signal-to-noise ratio (SNR), in which the noise is taken to be the local average amplitude calculated in a specified frequency range at the location of the pulsation mode in the frequency spectrum (see e.g. Kurtz et al. 2014; Bowman and Michielsen 2021).

In the case of coherent pulsation modes often seen in intermediate- and high-mass stars, the pulsation mode frequencies typically appear as Dirac-delta-like peaks with a full-width-half-maximum (FWHM) set by the Rayleigh resolution of the input time series. In other words, the pulsation mode lifetimes can be considered infinite relative to the length of the time series data, because the mode lifetime is not resolvable in time series data, even if it has a time span of a few decades. Once a significant coherent pulsation mode frequency has been identified, the optimal frequency, amplitude and phase can be determined by performing a least-squares fit of a multi-sinusoid function to the light curve using a model of the form

$$\Delta m = \sum_{i}^{N} A_i \sin(2\pi\nu_i(t - t_0) + \phi_i) \,, \tag{9}$$

where Δm is the model light curve with time stamps, t, and a pre-selected zero-point of the time series, t_0, and A_i are the amplitudes, ν_i are the frequencies, ϕ_i are the phases of the N significant frequencies included in the least-squares fit (Bowman and Michielsen, 2021). In practice, this process for coherent pulsators is called iterative prewhitening and is employed in a recursive manner, such that a single pulsation mode is identified as significant, optimised by least squares fitting, included in the model (c.f. Eqn. (9)), and then the model is subtracted from the light curve to create a residual light curve. After which the process repeats again such that when a new frequency spectrum is calculated on the next iteration all significant pulsation mode frequencies that came before it have been removed. All of the significant gravity-mode pulsations in the period spacing pattern of the SPB star KIC 7760680 are labelled in the frequency spectrum in Fig. 4. This also demonstrates that many of the gravity-mode frequencies are only marked as significant once the previous peaks have been removed during previous stages of iterative prewhitening — see discussion and application by Bowman and Michielsen (2021).

On the other hand, for stochastically excited pulsations, such as for SLOs, the pulsation modes have finite lifetimes making them resolvable in time series of several months or longer. This means the peaks of SLOs are broad and well represented by a Lorentzian, as can be seen in Fig. 3. Therefore, the application of iterative prewhitening described above does not apply to SLOs since their stochastically excited pulsations are not sufficiently periodic, such that they cannot be well represented by sinusoids in the time series data. In the case of SLOs, the use of Lorentzian functions as a direct fitting method can be automated with great speed and efficiency if mode identification is performed using an Echelle diagram to estimate $\Delta\nu$ a priori (e.g. Corsaro et al. 2020).

Once a list of all significant pulsation mode frequencies has been extracted via iterative prewhitening in the case of coherent pulsations or direct fitting using Lorentzians in the case of SLOs, the next step is to identify the spherical harmonic geometry of the modes (i.e. $\{n, \ell, m\}$). The best approach for this, however, depends on the type of pulsation mode, and the mass, evolutionary stage and pulsation excitation mechanism of the star. In general though, the methods for mode identification arise from applying the expectations from theory of how pulsation mode frequencies appear in a frequency spectrum such that numerical algorithms focused on pattern recognition have become increasingly more powerful and popular in the literature compared to visual inspection. The different methods of mode identification are generally specific to the type of pulsation modes, such as gravity modes, pressure modes, or mixed modes and their asymptotic properties creating regularity in period and/or frequency, for example period spacing patterns, rotational multiplets and Echelle diagrams, which were discussed in Section 2.

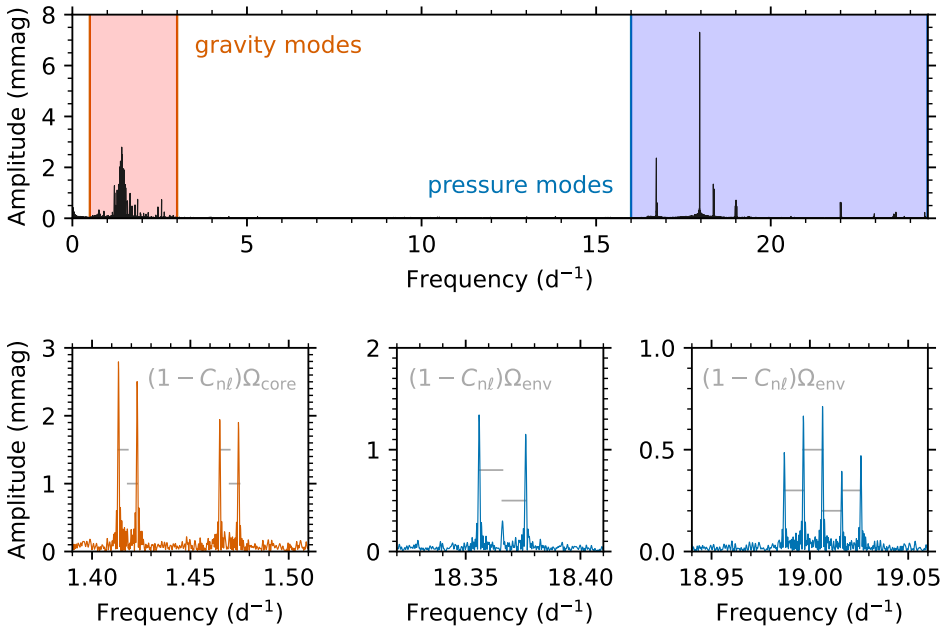

Fig. 5 Top Panel: Frequency spectrum of the δ Scuti star KIC 11145123 (Kurtz et al., 2014), in which the frequency regimes of gravity and pressure modes are denoted in red and blue, respectively. The bottom panels show zoom-ins of two gravity-mode dipole triplets ($\ell = 1$), a pressure-mode dipole triplet ($\ell = 1$), and a pressure-mode quintuplet ($\ell = 2$), from left-to-right. The frequency separation of components in a rotational multiplet reveals the rotation rate within the pulsation mode's cavity (cf. Eqn. 12).

3.2 Asteroseismic scaling relations

In the case of SLOs, once both $\Delta\nu$ and $\nu_{\rm max}$ (cf. Eqns. 3 and 4, respectively) have been identified, two simultaneous equations with two unknowns can be constructed, and rearranged to reveal the asteroseismic 'scaling relations' for mass and radius:

$$\frac{M}{M_\odot} \simeq \left(\frac{\nu_{\rm max}}{\nu_{\rm max,\odot}}\right)^3 \left(\frac{\Delta\nu}{\Delta\nu_\odot}\right)^{-4} \left(\frac{T_{\rm eff}}{T_{\rm eff,\odot}}\right)^{\frac{3}{2}}; \tag{10}$$

$$\frac{R}{R_\odot} \simeq \left(\frac{\nu_{\rm max}}{\nu_{\rm max,\odot}}\right)\left(\frac{\Delta\nu}{\Delta\nu_\odot}\right)^{-2} \left(\frac{T_{\rm eff}}{T_{\rm eff,\odot}}\right)^{\frac{1}{2}}, \tag{11}$$

where $\Delta\nu_\odot = 134.9$ Hz is the large frequency separation of the Sun. These scaling relations are extremely valuable for a simple but very precise estimate of fundamental parameters of solar-type and RGB stars (Hekker, 2020). The measurement of the surface gravity of the star $\left(g = \frac{GM}{R^3}\right)$ through asteroseismology and the application of the scaling relations in Eqns. (10) and (11) is the most precise for single stars. This precision then leads to important constraints on the age of a SLO, which is challenging to infer and yet highly relevant for many different fields of astrophysics (Chaplin and Miglio, 2013).

However, it is important to note that the asteroseismic scaling relations in Eqns. (10) and (11) do not include other stellar parameters, such as metallicity or other assumptions about the microphysics within a star, since they are normalised to observed properties of the Sun. Deviations from a constant frequency spacing in a frequency spectrum and Echelle diagram can be caused by rotation, or the presence of a chemical gradient and/or magnetic field within the pulsation cavity. Such effects may question the validity of the asteroseismic scaling relations for some stars, and a detailed asteroseismic study is then needed to properly constrain the physics responsible. On the other hand, the application of the asteroseismic scaling relations to infer masses and radii of tens of thousands of RGB stars has been used to investigate new aspects of physics within stellar interiors, as well as aid galactic archaeology (Chaplin and Miglio, 2013).

3.3 Measuring internal rotation

Since all stars rotate to some extent, the Coriolis force is important to consider for two main reasons. First, rotation breaks the assumption of spherical symmetry for stellar structure, because it 'flattens' a star making its equatorial radius larger than its polar radius. This leads to gravity darkening, such that the equator has a lower effective temperature than the pole (Kippenhahn et al., 2012; Langer, 2012). Second, rotation has a significant perturbative effect to pulsation mode frequencies through the Doppler shift. When combined, these two effects can drastically impact the excitation mechanisms of a pulsating star and the frequencies that are excited (Townsend, 2005; Szewczuk and Daszyńska-Daszkiewicz, 2017). For example, prograde (defined hereafter as $m > 0$) modes that travel in the direction of a star's rotation are imparted a positive Doppler shift to higher frequency, whereas retrograde (defined hereafter as $m < 0$) modes experience a Doppler shift

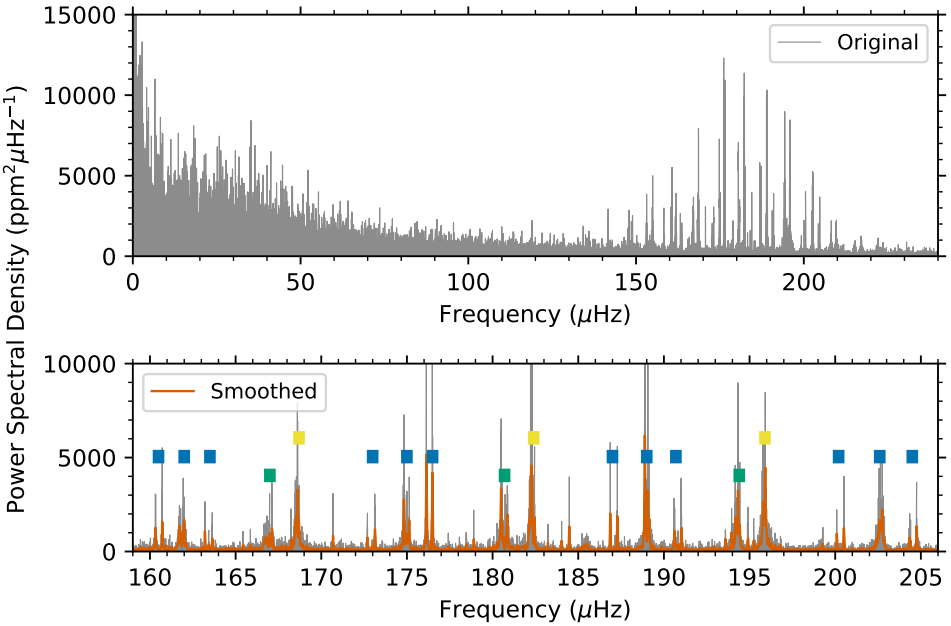

Fig. 6 Top Panel: Frequency spectrum of the pulsating RGB star KIC 8366239 (Beck et al., 2012), in which granulation from surface convection is dominant at low frequency, and the regular series of pulsation frequencies at high frequency can be seen. Bottom Panel: zoom-in of the pulsation frequencies, with radial ($\ell = 0$), rotationally-split dipole ($\ell = 1$) and quadruple ($\ell = 2$) modes marked by yellow, blue and green squares, respectively. The dipole modes are split by rotation into rotational multiplets.

to lower frequencies in the corotating reference frame of the star. Note that the observer is located in the inertial reference frame, meaning that the positive and negative frequency shifts for prograde and retrograde modes are mirrored when using the same azimuthal-order sign convention because of the change of reference frame (Aerts et al., 2010).

The simplest scenario is a star that is slowly rotating as a rigid body with a rotation rate of Ω, such that its radial rotation profile is constant. Slowly rotating here is defined as rotating at less than about 15% of its critical breakup velocity (Aerts, 2021). In such cases, a non-radial pulsation mode frequency, $\omega_{n\ell m}$, is given by:

$$\omega_{n\ell m} = \omega_{n\ell} + m(1 - C_{n\ell})\Omega, \tag{12}$$

where $C_{n\ell}$ is the Ledoux constant, and $\omega_{n\ell}$, is the degenerate (i.e. $m = 0$) pulsation mode frequency solution in the non-rotating scenario. The Ledoux constant takes a value of $0 \leq C_{n\ell} \leq 1$ and is dependent on the pulsation mode geometry and stellar structure (e.g. Burssens et al. 2023). However, a first-order approximation is that dipole pressure modes have $C_{n\ell} \simeq 0$, and dipole gravity modes have $C_{n\ell} \simeq 0.5$ (Aerts et al., 2010). Equation (12) gives rise to symmetric rotational multiplets in the frequency spectrum of a slowly-rotating star by lifting the degeneracy of pulsations modes of the same n and ℓ, but different m. Moreover, because of the quantum number selection rule of $-\ell \leq m \leq +\ell$, the number of component frequencies in a multiplet reveals the ℓ and corresponding m values. For example, a triplet corresponds to dipole (i.e. $\ell = 1$) pulsation modes separated into $m \in \{-1, 0, +1\}$, whereas a quintuplet corresponds to quadruple (i.e. $\ell = 2$) pulsation modes separated into $m \in \{-2, -1, 0, +1, +2\}$, and so on.

Rotational multiplets can exist for non-radial pressure and gravity modes, and are symmetic as long as the rotation rate is slow enough for the first-order approximation to apply (c.f. Eqn. 12), making them an effective method of mode identification (e.g. Aerts et al. 2003; Kurtz et al. 2014). For more rapidly stars, or stars with non-rigid radial rotation profiles, the first-order Ledoux approximation in Eqn. (12) is no longer valid and an higher-order formalism is required (Dziembowski and Goode, 1992; Suárez et al., 2010). Examples of slowly rotating pulsating stars with rotational multiplets are shown in Figs. 5 and 6. The former example is the main-sequence δ Scuti star KIC 11145123 studied by Kurtz et al. (2014), and was discovered to have a near-rigid radial rotation profile with a period of approximately 100 d. The latter example is the RGB star KIC 8366239 (Beck et al., 2012) which exhibits rotational splitting of approximately 0.3 μHz in its dipole mixed modes, as can be seen in its frequency spectrum in Fig. 6, which corresponds to a core-rotation period of about 40 d.

In addition to rotational multiplets, gravity-mode period spacing patterns are powerful diagnostic diagrams in gravity-mode asteroseismology for measuring interior rotation rates of pulsating stars, as introduced in Section 2.2. This is because high-radial order gravity-modes of consecutive radial order (n), but the same angular degree (ℓ) and azimuthal order (m), are equally spaced in period when plotted as a function of their pulsation period for a non-rotating and chemically homogeneous star. Rotation is a strong perturbation to pulsation periods through the Doppler shift, meaning that the Coriolis force induces a gradient in a gravity-mode period spacing pattern, with faster rotating stars having larger gradients (Bowman, 2020). Owing to the necessity of defining the observer to be in the inertial reference frame, prograde

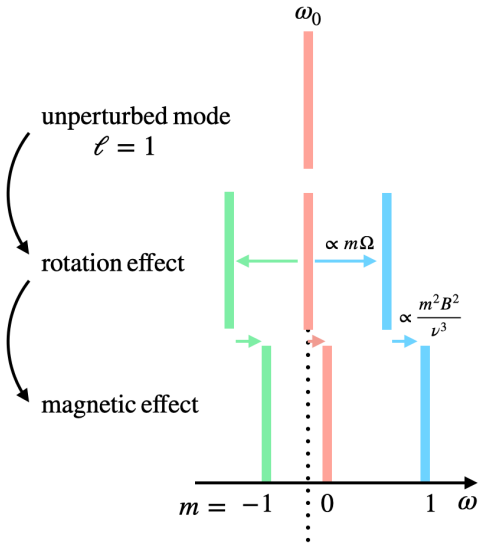

Fig. 7 Schematic effect of rotation and simple magnetic fields (at first order) on an gravity-mode frequency, lifting the degeneracy of the azimuthal order m of the mode and shifting the components to higher frequencies. Adapted from Bugnet et al. (2021).

pulsation modes (i.e. $m > 0$) have a negative gradient in a gravity-mode period spacing pattern. Whereas a retrograde (i.e. $m < 0$) period spacing pattern has positive gradient. Finally, the gradient of a zonal (i.e. $m = 0$) gravity-mode period spacing pattern is approximately zero, except for the fastest of rotators. Ensemble studies have revealed that prograde dipole (i.e. $\{\ell, m\} = \{1, 1\}$) gravity-mode period spacing patterns are by far the most common spherical harmonics geometry for pulsations in intermediate- and high-mass stars (Aerts, 2021).

3.4 Measuring internal magnetism

Magnetic fields also impact the structure of stars as well as the frequency of pulsations through the Lorentz force. Fortunately, the strength and geometry of interior magnetic fields can be probed with asteroseismology. In main-sequence stars with radiative envelopes, large-scale magnetic fields can significantly perturb gravity-mode pulsation frequencies (Hasan et al., 2005). During the RGB stage of evolution, mixed pressure-gravity mixed modes can be used to probe magnetic fields within their radiative cores (e.g. predictions by Loi, 2020; Bugnet et al., 2021). This is achieved by modelling the asymmetry magnetic fields induce in the asteroseismic signal. Indeed the frequency of mixed modes increases when the stellar interior is magnetized, and at first order gravity mode frequencies are perturbed following:

$$\omega_{n,\ell,m} \approx \omega_{n,\ell} + \frac{m^2 B^2}{\omega^3_{n,\ell}} \mathcal{R}_{n\ell}\,, \tag{13}$$

where B the strength of the radial component of the magnetic field at the hydrogen-burning shell, and $\mathcal{R}_{n\ell}$ is a factor that depends on the parameters of the star and the pulsation mode, akin to the Ledoux constant for rotation. Because of the m^2 dependency of the magnetic effect in Eqn. (13), the mixed mode pattern that is symmetric in the case of a rotating non-magnetized star becomes asymmetric, as shown in Fig. 7. The impact of the magnetic perturbation effect is most important at lower frequency for gravity modes due to the dependency in the term $1/\omega_{n,\ell}$ in Eqn. (13).

Internal magnetic fields in RGB stars were detected for the first time by Li et al. (2022) through the study of gravity-dominated mixed modes. This confirms the presence of strong magnetic fields in the cores of evolved low- and intermediate-mass stars. Previously this was postulated based on the observed suppressed amplitudes of mixed modes in such stars (Fuller et al., 2015; Stello et al., 2016). Magneto-asteroseismology has now become a very active field of research, aiming at evaluating the impact of magnetism on the internal dynamics and evolution of main-sequence stars (e.g. Lecoanet et al. 2022).

3.5 Forward asteroseismic modelling

The quantitative comparison of observed pulsation frequencies to those predicted from a multi-dimensional grid of theoretical stellar structure models is called forward asteroseismic modelling (Aerts et al., 2018; Aerts, 2021). In the typical forward asteroseismic modelling scenario, a grid of stellar models is computed for a particular type of pulsator or group of similar pulsators, since a dense grid of models covering the entire HR diagram is not feasible. These numerical models include a set of assumptions for the microphysics, such as opacities, chemical mixture, equation of state. The structure models contain free parameters to be determined, such as mass, initial hydrogen and metal mass fractions (i.e. X and Z), age, but also prescriptions for unconstrained physical processes such as chemical mixing. A stellar structure model grid is calculated to cover the required parameter space inferred from spectroscopic estimates of effective temperature and

luminosity, or surface gravity as a proxy, in the HR diagram, whilst varying the chosen free parameters.

The corresponding theoretical pulsation frequencies for each structure model in the grid are obtained by numerically perturbing the equilibrium structure models to calculate the Eigenfrequencies (e.g. Townsend et al. 2018) for a range spherical harmonic mode geometries. The parameter range to calculate is informed by observations, such as frequencies from frequency spectra and mode identification from rotational multiplets and/or gravity-mode period spacing patterns. Therefore, forward asteroseismic modelling is a model selection problem requiring a statistical framework (Aerts et al., 2018), such that the parameters of the best-fitting structure model are those that most accurately represent the physics of the observed star.

It is worth nothing that there are other approaches in asteroseismic modelling to constrain the interior physics of pulsating stars. For example, rotational and structural inversions (e.g. Bellinger et al. 2017; Vanlaer et al. 2023). There is also growing interest in the application of machine-learning techniques for efficient ensemble asteroseismic modelling (e.g. Mombarg et al. 2021).

4 Highlights from asteroseismology of different types of pulsating stars

In this section, we present an overview of important (and non-exhaustive) discussion of highlights from asteroseismology results in the last couple of decades. The majority of which are primarily thanks to long-term and high-precision light curves from space telescopes that provided the first continuous data sets spanning several years, such as the *Kepler* (2009-2014; Borucki et al. 2010) and ongoing TESS (Ricker et al., 2015) space missions.

Asteroseismology continues to expand to include a broad range of masses and evolutionary stages. New space photometry providing longer light curves allows higher frequency precision and allows us to probe different parameter spaces. An asteroseismic HR diagram is shown in Fig. 2, which contains many of the main types of pulsating stars — see Kurtz (2022). However, it is not possible to provide an exhaustive discussion of all pulsator types in this introductory chapter on Asteroseismology. The approximate ranges in effective temperature (and spectral type) and luminosity, typical pulsation periods and amplitudes for the main types of pulsators discussed in this chapter are provided in Table 1. A selection of example light curves to highlight the diversity in the variability amplitudes and time scales of pulsating stars are shown in Fig. 8, demonstrating the diversity in amplitudes and time scales of pulsating stars across the HR diagram.

4.1 Solar-type stars

Solar-type stars are main-sequence stars with a mass similar to that of the Sun ($0.8 \lesssim M \lesssim 1.3 M_{\odot}$). Owing to their similar structures they therefore also pulsate like the Sun, with stochastically excited pressure modes driven by turbulent convection in their convective envelopes (Chaplin and Miglio, 2013). Unfortunately, solar-type stars are typically quite faint in the Universe and their pulsation amplitudes are very small (i.e. $\sim$ ppm), making them challenging to detect and analyse. An excellent example of a pulsating solar-type star with a frequency spectra similar to the Sun is 16 Cyg A, which is shown in Fig. 3. In the specific application of seismology to the Sun – Helioseismology – a large fraction of the internal density and rotation profiles, as well as the depth of the convective envelope has been measured with great accuracy (Christensen-Dalsgaard et al., 1991).

4.2 Red giant branch (RGB) and red clump stars

RGB stars represent one of the future evolutionary stages of our Sun. Once the hydrogen is exhausted in the core at the end of main sequence, an intermediate- or low-mass star expands and eventually becomes a RGB star. Stochastically excited pulsations are commonly observed at the surfaces of RGBs stars. As their structures change as they ascend the RGB, the pulsations become more strongly coupled with gravity-mode pulsations in the deep radiative interior. As a result, it is typical to observe mixed modes for RGB stars (Chaplin and Miglio, 2013). Red clump stars are also giant stars, but they are in the core-helium burning phase which leads to pulsations with stronger signatures of having a mixed nature. Both RGB and red clump stars are broadly studied in asteroseismology, as the analysis of pulsation modes provide tight constraints on masses and radii via the asteroseismic scaling relations (cf. Eqn. (10) and (11)). Moreover, the mixed modes of RGB and red clump stars directly probe the physical processes of their deep interiors, which pressure modes alone in solar-type stars cannot achieve (Christensen-Dalsgaard et al., 1991). Recent breakthrough include statistics on the core rotation rates of thousands of RGB stars indicating that a strong angular momentum transport must be operating in the deep interior (e.g. Gehan et al. 2018), as well as the presence of strong magnetic fields in the cores of RGB stars (Li et al., 2022).

4.3 γ Dor stars

The γ Dor stars are main-sequence pulsators with spectral types between late-A and early-F, hence masses between about $1.5 \leq M \leq 2.5\,\mathrm{M}_{\odot}$. The high-radial order gravity modes in γ Dor stars are excited by a flux-blocking mechanism: the convective turnover timescale at the base of their thin surface convective envelopes is comparable to the pulsation periods of gravity modes, allowing a modulation of the outward flowing radiation sufficient to excite gravity modes (Guzik et al., 2000). This is similar to the opacity-driven heat-engine, except that it is the convective motions rather than opacity acting as the 'value' in the heat-engine of γ Dor stars. The gravity-mode period spacing patterns of γ Dor stars typically span a large range of radial orders and have been exploited to measure the near-core rotation rates for hundreds of stars (Van Reeth et al., 2016; Li et al., 2020). Forward asteroseismic modelling of gravity modes in ensembles of γ Dor stars has provided precise and accurate masses and ages, and demonstrated generally that the masses of the hydrogen-burning convective cores in such stars are underestimated by stellar evolution models and that additional mixing mechanisms is needed specifically at the core-envelope boundary layer (Mombarg et al., 2019). Moreover, the near-rigid radial rotation profiles and on average fast overall rotation rates of hundreds of γ Dor

Table 1 Properties of pulsator classes, including the name, a commonly acronym in the literature, mode type (where p=pressure, g=gravity and S=strange[a]), typical periods and photometric amplitudes, and the occupied parameter space in the HR diagram defined by ranges in effective temperature ($T_{\rm eff}$) and luminosity (L).

Pulsator Class Name	*Mode Type*	*Pulsation Periods*	*Pulsation Amplitudes*[bc]	$T_{\rm eff}$ *(K)*	L *($L_\odot$)*
Main Sequence					
Solar-type	p	1 – 10 min	few ppm	5000 – 6600	0.3 – 10
γ Dor	g	0.3 – 5 d	< 50 mmag	6500 – 9000	2 – 20
δ Sct	p,g	0.25 – 5 d	< 0.3 mag	6500 – 9000	3 – 100
roAp	p	5 – 22 min	< 10 mmag	6500 – 8500	5 – 30
SPB	g	0.5 – 5 d	< 50 mmag	11000 – 20000	$10^2 - 10^4$
Be	g	0.1 – 5 d	< 50 mmag	11000 – 30000	$10^2 - 10^4$
β Cep	p,g	0.05 – 3 d	< 50 mmag	15000 – 30000	$10^3 - 10^4$
SLF	g	0.01 – 10 d	< 50 mmag	10000 – 50000	$10^2 - 10^6$
Pre-Main Sequence					
T Tauri	p,g	0.05 – 5 d	< 5 mmag		
Herbig Ae/Be	p	1 – 8 hr	< 5 mmag		
Post-Main Sequence					
Red Giant Branch (RGB)	p,g	1 – 12 hr	10 – 100 ppm	4500 – 5000	0.3 – 100
RR Lyr	p	0.3 – 0.5 d	< 1.5 mag	6000 – 8000	25 – 50
Type II Cepheid (W Vir)	p	10 – 30 d	< 1 mag	5000 – 8000	$10^2 - 10^4$
Type II Cepheid (BL Her)	p	1 – 5 d	< 1 mag	5000 – 8000	$10^2 - 10^4$
Type I Cepheid	p	1 – 50 d	< 1 mag	3500 – 7000	$10^2 - 10^{5.5}$
RV Tauri	p	30 – 150 d	< 3 mag	4000 – 8000	$10^{3.2} - 10^{4.2}$
Mira (SRa, SRb, SRc)	p	> 80 d	< 8 mag	2800 – 5600	$10^{2.5} - 10^{4.0}$
Mira (SRd)	p	< 80 d	< 1 mag	2800 – 5600	$10^{2.5} - 10^{4.0}$
α Cyg	g,S?	10 – 100 d	< 0.3 mag	2800 – 10000	$10^{2.5} - 10^{4.5}$
S Dor / LBV	g,S	2 – 40 d	< 0.1 mag	6300 – 16000	$10^{5.5} - 10^{6.5}$
sdBV	p	80 – 800 sec	< 0.1 mag	15000 – 30000	15 – 150
sdBV	g	0.5 – 3 hr	< 10 mmag	25000 – 40000	15 – 400
GW Vir / DOV	g	5 – 80 min	< 0.2 mag	60000 – 120000	30 – 3000
V777 Her / DBV	g	2 – 16 min	< 0.2 mag	25000 – 40000	0.1 – 5
ZZ Ceti / DAV	g	0.5 – 25 min	< 0.2 mag	9000 – 14000	$10^{-2.6} - 10^{-2.2}$
R CrB	g?	40 – 100 d	< 50 mmag	3100 – 16000	$10^{3.5} - 10^{4.5}$
PV Tel	S	~ 20 d	< 50 mmag	3100 – 16000	$10^{3.5} - 10^{4.5}$
V652 Her	g,S?	~ 0.1 d	< 50 mmag	3100 – 16000	$10^{3.5} - 10^{4.5}$

[a]Strange modes are theoretically predicted for massive stars near the Eddington limit (i.e. large L/M ratios) and are non-linear radial instabilities caused by the strong enhancements in the non-adiabatic partial ionization zones of helium and heavy elements, resulting in long period and high-amplitude outburst-like pulsations (Glatzel et al., 1999; Aerts et al., 2010).

[b]The units here are photometric pulsation amplitudes and are expressed in the most common form used in the literature for each pulsator class, with an approximate conversion being: $1\mu{\rm mag} \simeq 1$ ppm.

[c]Pulsations amplitudes are those typically observed in broadband optical photometry, but in reality these depend on the colour of the star and the wavelength passband of the instrument. Note also that spectroscopic amplitudes of pulsations can differ to their photometric counterparts although they are generally less available in the literature.

stars are currently a challenge to explain with current angular momentum transport theory (Ouazzani et al., 2019).

4.4 δ Sct stars

The δ Sct stars have spectral types of A and early-F, and masses between about $1.5 \leq M \leq 3$ M$_\odot$. They lie at the intersection of the main-sequence and the classical Cepheid instability strip in the HR diagram, and span the pre-main sequence (e.g. Zwintz et al. 2014) to the post-main sequence (Breger, 2000). The heat-engine mechanism operating in the helium partial ionisation zone at 50 000 K is efficient in exciting low-radial order pressure modes with periods spanning from several hours up to tens of minutes (Breger, 2000). The majority, but not all, of δ Sct stars are also observed to have gravity-mode pulsations with periods between a few days and several hours making δ Sct stars commonly hybrid pulsators (e.g. Uytterhoeven et al. 2011), which models struggle to explain. The small fraction of δ Sct stars with higher-frequency pressure modes with periods of order tens of minutes are thought to be excited by turbulent pressure (Antoci et al., 2019). Given their often hybrid nature, the use of rotational multiplets in slowly rotating δ Sct stars allows the radial rotation profile to be extracted. Kurtz et al. (2014) demonstrated KIC 11145123 to have a nearly uniform interior rotation period of approximately 100 d, which is shown in Fig. 5. However, the δ Sct stars are often rapid rotators making their frequency spectra complex and difficult to interpret and forward asteroseismic modelling challenging (Daszyńska-Daszkiewicz et al., 2021). Some δ Sct stars show regular patterns in their frequency spectra (e.g. Bedding et al. 2020), allowing the application of Echelle diagrams for mode identification and forward asteroseismic

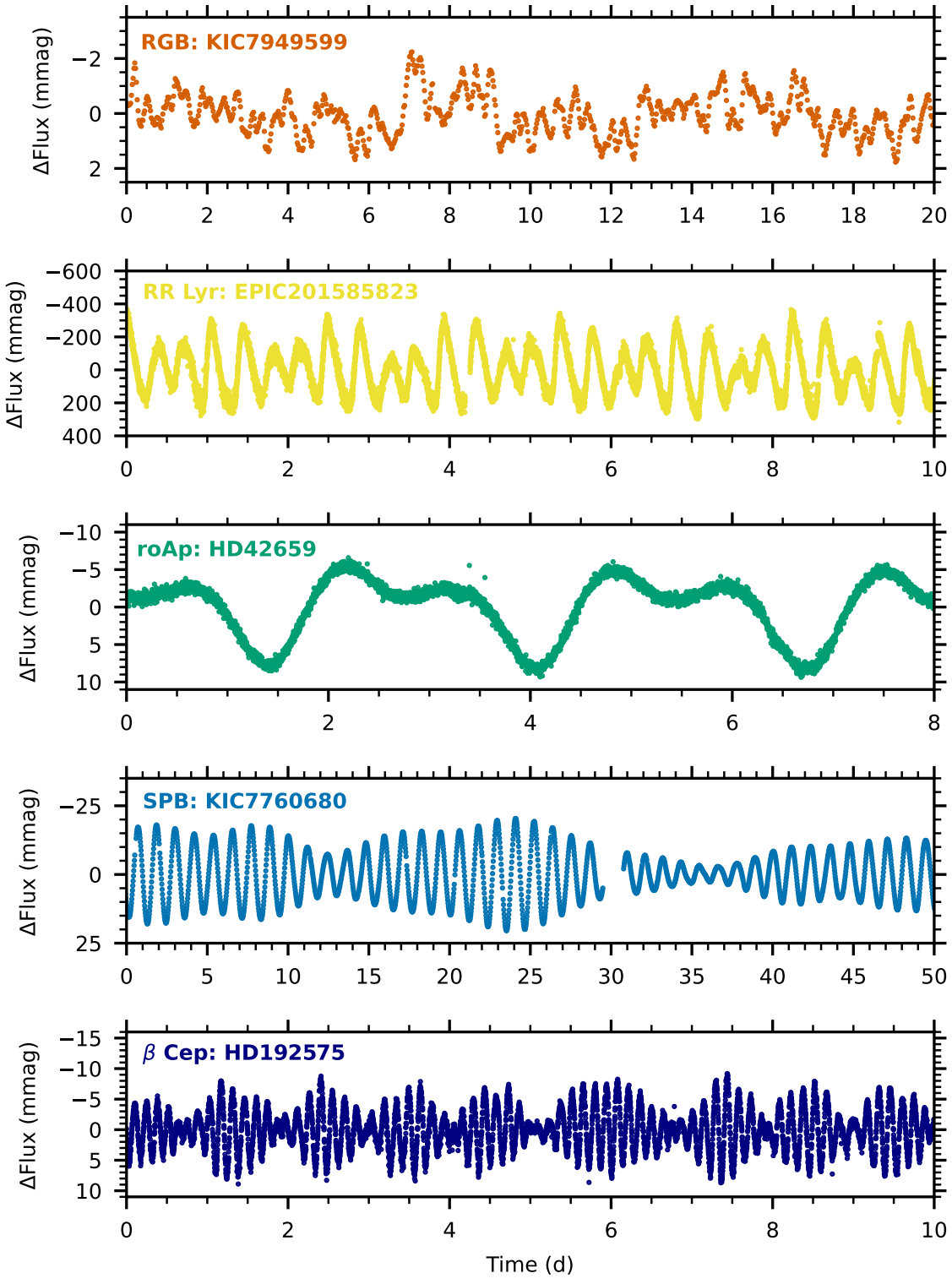

Fig. 8 Example light curves of a selection of different types of pulsating stars discussed in Section 4. Note that the ordinate and abscissa scales are not the same because of the different peak-to-peak brightness and timescales caused by pulsations among the selected pulsator classes.

modelling (Panda et al., 2024).

4.5 roAp stars

The rapidly oscillating Ap (roAp) stars are a sub-group of chemically-peculiar pulsating A-type stars located near the main sequence within the classical instability strip (Cunha, 2002). They have strong dipolar magnetic fields, slow rotation rates, and high-radial order and low-angular degree magneto-acoustic pulsation modes with periods of order several minutes (Kurtz, 1990). The exact pulsation excitation mechanism(s) at work in roAp stars is not fully understood, but it is likely a combination of the heat-engine mechanism operating in the hydrogen partial ionisation zone and turbulent pressure (Cunha et al., 2013). The strong magnetic field within a roAp star is typically misaligned with respect to the rotation and pulsation axes, which gives rise to the oblique pulsator model (Kurtz, 1982). This allows the pulsations to be viewed from different orientations as the star rotates, giving rise to rotational multiplets in their frequency spectra. Only about 100 roAp stars are known making them a particularly rare type of pulsating star (Holdsworth et al., 2024).

4.6 RR Lyrae stars

RR Lyrae (RR Lyr) stars are often referred to as classical pulsators because of their dominant high-amplitude radial-mode pulsations caused by the heat-engine mechanism, and they have been used historically as standard candles in astrophysics. They are metal-poor and old (i.e. Population II) giant stars with masses smaller than about 1 $M_\odot$ on the horizontal branch (Aerts et al., 2010). RR Lyr stars are subdivided into RRab and RRc stars, with the former classified by having highly non-sinusoidal light curves caused predominantly by non-linear behaviour in the fundamental radial pulsation mode, whereas RRc stars have sinusoidal light curves dominated by the first-overtone radial mode (Stellingwerf, 1975). Some RR Lyr stars are not perfectly periodic and exhibit a form of amplitude and phase modulation called the Blazhko effect (Blažko, 1907). Another phenomenon found in RR Lyr stars is period doubling which is caused by half-integer resonances (e.g. 3:2, 9:2) among the overtone and fundamental radial modes (Moskalik and Buchler, 1990). In a light curve, period doubling appears as alternating minima and maxima in the brightness excursions (Szabó et al., 2014).

4.7 Cepheid variables

Cepheid variables are also known as classical pulsators from their heat-engine radial-mode pulsations and from being standard candles. They are evolved horizontal branch stars crossing the classical instability strip in the HR diagram (Aerts et al., 2010). Cepheids are subdivided into two groups. Type I Cepheids are Population I stars crossing the classical instability strip for the first time, have radial-mode pulsations with periods between 1 and 50 d. The period ratios of first-overtone and fundamental radial modes elucidate their evolutionary age (Petersen, 1973). Type II Cepheids are Population II stars transitioning from the horizontal branch to the asymptotic giant branch (Wallerstein, 2002). They also pulsate in radial modes, but are subdivided into three classes because they have heterogeneous pulsation periods: BL Herculis stars have periods between 1 and 5 d; W Virginis stars have periods between 10 and 20 d; and RV Tauri stars have periods longer than 20 d (Aerts et al., 2010).

4.8 SPB and Be stars

The slowly pulsating B-type (SPB) stars are dwarf stars with spectral types between B3 and B9, and have high-radial order gravity modes excited by the heat-engine mechanism operating in the iron-bump at 200 000 K (Dziembowski and Pamyatnykh, 1993; Pamyatnykh, 1999). Forward asteroseismic modelling of their gravity-mode period spacing patterns has revealed their near-core rotation rates (Pápics et al., 2017; Szewczuk et al., 2021) as well as a diversity in the amount of interior mixing (Pedersen et al., 2021). The frequency spectrum and gravity-mode period spacing pattern of the SPB star KIC 7760680 is shown in Fig. 4. Interestingly, a handful of SPB stars host a strong large-scale magnetic field at their surfaces (e.g. Buysschaert et al. 2018). Through a combination of spectropolarimetry, asteroseismology and MHD simulations, this has allowed magneto-asteroseismology to probe the strength of the magnetic field in the deep interior near the convective core in the SPB star HD 43317 (Lecoanet et al., 2022). The analysis suggests the presence of a core-dynamo strengthening the large-scale fossil field. Finally, about 20% of dwarf B-type stars rotate sufficiently rapidly to create a so-called decretion disk of ejected circumstellar material and be classified as Be stars (Rivinius et al., 2013). The signature of rapid rotation and a decretion disk is made based on observing strong emission lines in spectroscopy, which are also known to be time-dependent. The Be stars are commonly found to pulsate, with rotation rate and pulsator fraction being correlated (Labadie-Bartz et al., 2022). The rapid rotation and pulsations provide very efficient angular momentum transport and chemical mixing (Huat et al., 2009; Neiner et al., 2020).

4.9 β Cep stars

The β Cephei stars are massive stars with spectral types typically ranging between late-O and early-B whilst on the main sequence, thus they have birth masses between approximately 8 and 30 $M_\odot$ (Bowman, 2020). The heat-engine mechanism is efficient in exciting low-radial order pressure and gravity modes with periods of order several hours (Dziembowski et al., 1993; Pamyatnykh, 1999). Space photometry from the TESS mission has demonstrated that β Cep stars are fairly common and there may be no upper mass limit for these stars (Burssens et al., 2020). Historically, the high-amplitude pulsations observed using ground-based telescopes for a handful of β Cep stars have proven extremely fruitful in constraining their interior rotation profiles (e.g. Aerts et al. 2003; Dupret et al. 2004). With modern space telescopes and more sophisticated forward asteroseismic modelling, the precision on mass, age, rotation and mixing that is achievable has much improved in recent years (Burssens et al., 2023).

4.10 SLF variability

The now-retired *Kepler* and ongoing TESS space missions have revealed that almost all massive stars exhibit a non-periodic form of variability known as stochastic low-frequency (SLF) variability (Bowman et al., 2019). It is characterised by power excess in a frequency spectrum with amplitudes ranging from micro-magnitudes to milli-magnitudes, and a broad period range from several days to minutes. Although, the physical mechanism for SLF variability is not firmly established, there are two non-mutually exclusive mechanisms: stochastically excited gravity waves (i.e. damped gravity modes with finite lifetimes) from the convective core or sub-surface convection zones (Bowman, 2023). Regardless of excitation mechanism, the excited damped pulsations have been shown to probe a massive star's mass and age (Bowman et al., 2020), and permits wave asteroseismology of massive stars that do not have the high-amplitude heat-driven coherent pulsation modes.

4.11 Subdwarf stars

The subdwarf B (sdB) stars are low-luminosity B-type stars with masses less than about 0.5 $M_{\odot}$, and are in an unusual stage of evolution because they have experienced significant mass loss as an RGB star to leave behind a helium core (Aerts et al., 2010). They are located between the RGB and the extreme horizontal branch in the HR diagram and are progenitors of white dwarf stars. The discovery of their pulsational properties is fairly recent (Kilkenny et al., 1997), with a growing number of variable sdB (i.e. sdBV) stars grouped into whether they are dominated by pressure or gravity modes. The gravity-mode sdB stars are cooler than the pressure-mode sdB stars, making them analogous to SPB and β Cep stars, respectively. The pulsations in sdB stars are excited by the heat-engine mechanism, and are commonly low-radial order and low-angular degree (Kilkenny, 2007). Asteroseismology of sdB stars has revealed tight constraints on their interior rotation (Charpinet et al., 2018), as well as their masses and ages (e.g. Charpinet et al. 2006, 2019; Zong et al. 2016).

4.12 White dwarfs

Eventually all low- and intermediate-mass stars become white dwarf stars, with the white dwarf cooling track shown in Fig. 2. Spectroscopic studies of white dwarfs divide them into three main spectral class regimes of DA, DB, and DO, which have since all been discovered to contain pulsations (Aerts et al., 2010). From hottest to coolest, these are: variable DO stars (i.e. DOV; also known as GW Vir stars); variable DB stars (i.e. DBV; also known as V777 Her stars); and variable DA stars (i.e. DAV; also known as ZZ Cet stars). Pulsations in white dwarfs are excited by the heat-engine mechanism, although it is sometime referred to as convective driving in the literature for DAV stars (e.g. Brickhill 1991). Pulsations in white dwarfs are low-angular degree pressure and/or gravity modes based on their spectral type, and typically have short pulsation periods owing to their high densities — see reviews by Fontaine and Brassard (2008) and Winget and Kepler (2008). Asteroseismology of white dwarfs has revealed their interior rotation (Hermes et al., 2017) and chemical composition profiles to great precision (e.g. Giammichele et al. 2018; Charpinet et al. 2019).

5 Conclusions

Asteroseismology is a relatively new sub-field within stellar astrophysics, but it is growing rapidly in depth and breadth year on year. This advancement has been driven by the space photometry revolution in the last two decades, such as from the *Kepler* (Borucki et al., 2010) and TESS (Ricker et al., 2015) space telescopes, which have provided high-photometric precision and long-duration light curves for hundreds of thousands of stars. With improved data quality and quantity, which is orders of magnitudes better than the best cases previously achieved from the ground, asteroseismology has been applied to tens of thousands of RGB stars (Chaplin and Miglio, 2013), several hundred main-sequence pulsators and dozens of compact objects like white dwarfs and subdwarfs (Aerts, 2021; Kurtz, 2022). In so doing, asteroseismology has provided some of the most precise measurements of fundamental stellar parameters, such as masses, radii and ages, as well as accurate constraints on interior physical processes such as rotation and mixing mechanisms.

One of the most important conclusions of asteroseismology having been applied across several different types of pulsators, which includes high-mass and intermediate-mass dwarfs, evolved low-mass and intermediate-mass stars, as well as white dwarfs and subdwarfs, is that all stars have a smaller amount of radial differential rotation than expected from theory (Aerts et al., 2019). The vast majority of stars for which asteroseismology using gravity-mode period-spacing patterns and/or rotational multiplets has revealed similar (near-)core and envelope rotation rates. Observed core-to-surface rotation ratios range approximately between 1-10, whereas models predicted values at an order of magnitude larger than this for all types of stars (Aerts et al., 2019; Aerts, 2021). This means that a very efficient angular momentum transport mechanism, which remains challenging to explain (Townsend et al., 2018; Ouazzani et al., 2019), must be operating during most of a star's lifetime for a wide range of masses. This is because the sample of asteroseismic interior rotation rates include thousands of stars spanning the core-hydrogen, shell-hydrogen, core-helium evolutionary stages and beyond and all seem to show similar results (Aerts, 2021). On the other hand, asteroseismic interior rotation profiles for massive stars are few in number compared to low- and intermediate-mass stars, primarily because their rapid rotation, high binary fraction, and intrinsic scarcity in the Universe make them challenging to study (Bowman, 2020; Burssens et al., 2023). The strong missing angular momentum transport mechanism revealed by asteroseismology is an impactful conclusion for the wider astrophysics community. Inaccurate interior rotation profiles and unconstrained efficiencies in angular momentum transport mechanisms lead to uncalibrated interior chemical mixing processes in stellar evolution models, which limits our ability to reliably estimate stellar masses and ages. Leading explanations for the missing angular momentum transport mechanism(s) are magnetic fields and non-radial pulsations, both of which have shown great promise but are not mutually exclusive (Aerts et al., 2019).

In parallel to time-series space photometry surveys, other impactful projects within astrophysics include ESA's GAIA mission (Gaia Collaboration et al., 2016) and large-scale ground-based spectroscopic campaigns and are providing highly complementary data for constraining

fundamental parameters. Ultra-precise parallaxes from GAIA combined with accurate spectroscopic constraints on effective temperatures allows stars to be robustly placed in the HR diagram, which greatly aids asteroseismic analysis. In the near future, ESA's PLATO mission, with a planned launch date in 2026 (Rauer et al., 2024), will greatly build on the previous *Kepler* and ongoing TESS missions by providing high-precision and long-duration light curves of millions of stars across the sky. The advantageous synergy between asteroseismology and the study of exoplanets, and the golden age of asteroseismology is expected to continue and reach new heights in the coming decades.

Summary of Key Points

1. Stellar pulsations are described in terms of spherical harmonic geometry, with a given pulsation mode frequency having a unique radial order (n), angular degree (ℓ), and azimuthal order (m).
2. Long-duration, high-precision, continuous time-series data are required to unambiguously identify pulsation mode frequencies, and measure diagnostics such as gravity-mode period spacing patterns, and rotationally- and magnetically-split pulsation multiplets.
3. Pulsations are commonplace across the HR diagram, and a diverse range of variability, including binarity, rotation, and pulsations allows asteroseismology to study the physics of stellar interiors.
4. Asteroseismology provides precise constraints on interior physics of stars, such as rotation, mixing and magnetic fields, as well as fundamental parameters such as masses, radii and ages.
5. Most stars are observed to have only a small amount of radial differential rotation, meaning an efficient angular momentum transport mechanism operates throughout stellar evolution that is currently uncalibrated in stellar evolution models.
6. Direct insight of the strength and geometry of magnetic fields deep inside main-sequence and evolved stars is now possible thanks to magneto-asteroseismology.

Acknowledgments

DMB gratefully acknowledges funding from UK Research and Innovation (UKRI) in the form of a Frontier Research Grant under the UK government's ERC Horizon Europe funding guarantee (SYMPHONY; grant number: EP/Y031059/1), and a Royal Society University Research Fellowship (URF; grant number: URF\R1\231631). The authors are grateful to C. S. Jeffrey for generously making Fig. 2. The *Kepler* and TESS data presented in this paper were obtained from the Mikulski Archive for Space Telescopes (MAST; `https://archive.stsci.edu/`) at the Space Telescope Science Institute (STScI), which is operated by the Association of Universities for Research in Astronomy, Inc., under NASA contract NAS5-26555. Support to MAST for these data is provided by the NASA Office of Space Science via the grants NAG5-7584 and NNX09AF08G, and other grants and contracts. Funding for the TESS mission is provided by the NASA Explorer Program, and funding for the *Kepler* and K2 missions was provided by NASA's Science Mission Directorate.

References

Aerts C (2021), Jan. Probing the interior physics of stars through asteroseismology. *Reviews of Modern Physics* 93 (1), 015001. doi:10.1103/RevModPhys.93.015001.

Aerts C, Thoul A, Daszyńska J, Scuflaire R, Waelkens C, Dupret MA, Niemczura E and Noels A (2003), Jun. Asteroseismology of HD 129929: Core Overshooting and Nonrigid Rotation. *Science* 300: 1926–1928. doi:10.1126/science.1084993.

Aerts C, Christensen-Dalsgaard J and Kurtz DW (2010). Asteroseismology, Springer.

Aerts C, Molenberghs G, Michielsen M, Pedersen MG, Björklund R, Johnston C, Mombarg JSG, Bowman DM, Buysschaert B, Pápics PI, Sekaran S, Sundqvist JO, Tkachenko A, Truyaert K, Van Reeth T and Vermeyen E (2018), Jul. Forward Asteroseismic Modeling of Stars with a Convective Core from Gravity-mode Oscillations: Parameter Estimation and Stellar Model Selection. 237, 15. doi:10.3847/1538-4365/aaccfb. 1806.06869.

Aerts C, Mathis S and Rogers TM (2019), Aug. Angular Momentum Transport in Stellar Interiors. *Ann. Rev. Astron. Astrophys.* 57: 35–78. doi:10.1146/annurev-astro-091918-104359. 1809.07779.

Antoci V, Cunha MS, Bowman DM, Murphy SJ, Kurtz DW, Bedding TR, Borre CC, Christophe S, Daszyńska-Daszkiewicz J, Fox-Machado L, García Hernández A, Ghasemi H, Handberg R, Hansen H, Hasanzadeh A, Houdek G, Johnston C, Justesen AB, Kahraman Alicavus F, Kotysz K, Latham D, Matthews JM, Mønster J, Niemczura E, Paunzen E, Sánchez Arias JP, Pigulski A, Pepper J, Richey-Yowell T, Safari H, Seager S, Smalley B, Shutt T, Sódor A, Suárez JC, Tkachenko A, Wu T, Zwintz K, Barceló Forteza S, Brunsden E, Bognár Z, Buzasi DL, Chowdhury S, De Cat P, Evans JA, Guo Z, Guzik JA, Jevtic N, Lampens P, Lares Martiz M, Lovekin C, Li G, Mirouh GM, Mkrtichian D, Monteiro MJPFG, Nemec JM, Ouazzani RM, Pascual-Granado J, Reese DR, Rieutord M, Rodon JR, Skarka M, Sowicka P, Stateva I, Szabó R and Weiss WW (2019), Dec. The first view of δ Scuti and γ Doradus stars with the TESS mission. *MNRAS* 490 (3): 4040–4059. doi:10.1093/mnras/stz2787. 1909.12018.

Beck PG, Montalban J, Kallinger T, De Ridder J, Aerts C, García RA, Hekker S, Dupret MA, Mosser B, Eggenberger P, Stello D, Elsworth Y, Frandsen S, Carrier F, Hillen M, Gruberbauer M, Christensen-Dalsgaard J, Miglio A, Valentini M, Bedding TR, Kjeldsen H, Girouard FR, Hall JR and Ibrahim KA (2012), Jan. Fast core rotation in red-giant stars as revealed by gravity-dominated mixed modes. *Nature* 481: 55–57. doi:10.1038/nature10612. 1112.2825.

Bedding TR, Mosser B, Huber D, Montalbán J, Beck P, Christensen-Dalsgaard J, Elsworth YP, García RA, Miglio A, Stello D, White TR, De Ridder J, Hekker S, Aerts C, Barban C, Belkacem K, Broomhall AM, Brown TM, Buzasi DL, Carrier F, Chaplin WJ, di Mauro MP, Dupret MA, Frandsen S, Gilliland RL, Goupil MJ, Jenkins JM, Kallinger T, Kawaler S, Kjeldsen H, Mathur S, Noels A, Silva Aguirre V and Ventura P (2011), Mar. Gravity modes as a way to distinguish between hydrogen- and helium-burning red giant stars. *Nature* 471: 608–611. doi:10.1038/nature09935. 1103.5805.

Bedding TR, Murphy SJ, Hey DR, Huber D, Li T, Smalley B, Stello D, White TR, Ball WH, Chaplin WJ, Colman IL, Fuller J, Gaidos E, Harbeck DR, Hermes JJ, Holdsworth DL, Li G, Li Y, Mann AW, Reese DR, Sekaran S, Yu J, Antoci V, Bergmann C, Brown TM, Howard AW, Ireland MJ, Isaacson H, Jenkins JM, Kjeldsen H, McCully C, Rabus M, Rains AD, Ricker GR, Tinney CG and Vanderspek RK (2020), May. Very regular high-frequency pulsation modes in young intermediate-mass stars. *Nature* 581 (7807): 147–151. doi:10.1038/s41586-020-2226-8. 2005.06157.

Bellinger EP, Basu S, Hekker S and Ball WH (2017), Dec. Model-independent Measurement of Internal Stellar Structure in 16 Cygni A and B. *ApJ* 851, 80. doi:10.3847/1538-4357/aa9848. 1710.11487.

Blažko S (1907), Aug. Mitteilung über veränderliche Sterne. *Astronomische Nachrichten* 175: 325. doi:10.1002/asna.19071752002.

Borucki WJ, Koch D, Basri G, Batalha N, Brown T, Caldwell D, Caldwell J, Christensen-Dalsgaard J, Cochran WD, DeVore E, Dunham EW, Dupree AK, Gautier TN, Geary JC, Gilliland R, Gould A, Howell SB, Jenkins JM, Kondo Y, Latham DW, Marcy GW, Meibom S, Kjeldsen H, Lissauer JJ, Monet DG, Morrison D, Sasselov D, Tarter J, Boss A, Brownlee D, Owen T, Buzasi D, Charbonneau D, Doyle L, Fortney J, Ford EB, Holman MJ, Seager S, Steffen JH, Welsh WF, Rowe J, Anderson H, Buchhave L, Ciardi D, Walkowicz L, Sherry W, Horch E, Isaacson H, Everett ME, Fischer D, Torres G, Johnson JA, Endl M, MacQueen P, Bryson ST, Dotson J, Haas M, Kolodziejczak J, Van Cleve J, Chandrasekaran H, Twicken JD, Quintana EV, Clarke BD, Allen C, Li J, Wu H, Tenenbaum P, Verner E, Bruhweiler F, Barnes J and Prsa A (2010), Feb. Kepler Planet-Detection Mission: Introduction and First Results. *Science* 327: 977–. doi:10.1126/science.1185402.

Bowman DM (2020), Oct. Asteroseismology of high-mass stars: new insights of stellar interiors with space telescopes. *Frontiers in Astronomy and Space Sciences* 7, 70. doi:10.3389/fspas.2020.578584. 2008.11162.

Bowman DM (2023), Dec. Making waves in massive star asteroseismology. *Astrophys. Space Sci.* 368 (12), 107. doi:10.1007/s10509-023-04262-7. 2312.08319.

Bowman DM and Michielsen M (2021), Dec. Towards a systematic treatment of observational uncertainties in forward asteroseismic modelling of gravity-mode pulsators. *A&A* 656, A158. doi:10.1051/0004-6361/202141726. 2109.10776.

Bowman DM, Burssens S, Pedersen MG, Johnston C, Aerts C, Buysschaert B, Michielsen M, Tkachenko A, Rogers TM, Edelmann PVF, Ratnasingam RP, Simón-Díaz S, Castro N, Moravveji E, Pope BJS, White TR and De Cat P (2019), May. Low-frequency gravity waves in blue supergiants revealed by high-precision space photometry. *Nature Astronomy* 3: 760–765. doi:10.1038/s41550-019-0768-1. 1905.02120.

Bowman DM, Burssens S, Simón-Díaz S, Edelmann PVF, Rogers TM, Horst L, Röpke FK and Aerts C (2020), Aug. Photometric detection of internal gravity waves in upper main-sequence stars. II. Combined TESS photometry and high-resolution spectroscopy. *A&A* 640, A36. doi:10.1051/0004-6361/202038224. 2006.03012.

Breger M (2000), δ Scuti stars (Review), Breger M and Montgomery M, (Eds.), Delta Scuti and Related Stars, Astronomical Society of the Pacific Conference Series, 210, pp. 3.

Brickhill AJ (1991), Aug. The pulsations of ZZ Ceti stars. III - The driving mechanism. *MNRAS* 251: 673–680. doi:10.1093/mnras/251.4.673.

Bugnet L, Prat V, Mathis S, Astoul A, Augustson K, García RA, Mathur S, Amard L and Neiner C (2021), Jun. Magnetic signatures on mixed-mode frequencies. I. An axisymmetric fossil field inside the core of red giants. *A&A* 650, A53. doi:10.1051/0004-6361/202039159. 2102.01216.

Burssens S, Simón-Díaz S, Bowman DM, Holgado G, Michielsen M, de Burgos A, Castro N, Barbá RH and Aerts C (2020), Jul. Variability of OB stars from TESS southern Sectors 1-13 and high-resolution IACOB and OWN spectroscopy. *A&A* 639, A81. doi:10.1051/0004-6361/202037700. 2005.09658.

Burssens S, Bowman DM, Michielsen M, Simón-Díaz S, Aerts C, Vanlaer V, Banyard G, Nardetto N, Townsend RHD, Handler G, Mombarg JSG, Vanderspek R and Ricker G (2023), Aug. A calibration point for stellar evolution from massive star asteroseismology. *Nature Astronomy* 7: 913–930. doi:10.1038/s41550-023-01978-y. 2306.11798.

Buysschaert B, Aerts C, Bowman DM, Johnston C, Van Reeth T, Pedersen MG, Mathis S and Neiner C (2018), Sep. Forward seismic modeling of the pulsating magnetic B-type star HD 43317. *A&A* 616, A148. doi:10.1051/0004-6361/201832642. 1805.00802.

Chaplin WJ and Miglio A (2013), Aug. Asteroseismology of Solar-Type and Red-Giant Stars. *Ann. Rev. Astron. Astrophys.* 51: 353–392. doi:10.1146/annurev-astro-082812-140938. 1303.1957.

Charpinet S, Silvotti R, Bonanno A, Fontaine G, Brassard P, Chayer P, Green EM, Bergeron P, Bernabei S, Leccia S, Kjeldsen H, Janulis R, Frasca A, Østensen R, Kim SL, Park BG, Jiang X, Reed MD, Patterson RS, Gietzen KM, Clark PJ, Wolf GW, Lipkin Y, Formiggini L, Leibowitz E, Oswalt TD, Rudkin M and Johnston K (2006), Nov. The rapidly pulsating subdwarf B star PG 1325+101. II. Structural parameters from asteroseismology. *A&A* 459: 565–576. doi:10.1051/0004-6361:20065316.

Charpinet S, Giammichele N, Zong W, Van Grootel V, Brassard P and Fontaine G (2018), Jul. Rotation in sdB stars as revealed by stellar oscillations. *Open Astronomy* 27 (1): 112–119. doi:10.1515/astro-2018-0012.

Charpinet S, Brassard P, Fontaine G, Van Grootel V, Zong W, Giammichele N, Heber U, Bognár Z, Geier S, Green EM, Hermes JJ, Kilkenny D, Østensen RH, Pelisoli I, Silvotti R, Telting JH, Vučković M, Worters HL, Baran AS, Bell KJ, Bradley PA, Debes JH, Kawaler SD, Kołaczek-Szymański P, Murphy SJ, Pigulski A, Sódor À, Uzundag M, Handberg R, Kjeldsen H, Ricker GR and Vanderspek RK (2019), Dec. TESS first look at evolved compact pulsators. Discovery and asteroseismic probing of the g-mode hot B subdwarf pulsator EC 21494-7018. *A&A* 632, A90. doi:10.1051/0004-6361/201935395. 1910.04234.

Christensen-Dalsgaard J, Gough DO and Thompson MJ (1991), Sep. The Depth of the Solar Convection Zone. *ApJ* 378: 413. doi:10.1086/170441.

Corsaro E, McKeever JM and Kuszlewicz JS (2020), Aug. Fast and Automated Peak Bagging with DIAMONDS (FAMED). *A&A* 640, A130. doi:10.1051/0004-6361/202037930. 2006.08245.

Cunha MS (2002), Jun. A theoretical instability strip for rapidly oscillating Ap stars. *MNRAS* 333: 47–54. doi:10.1046/j.1365-8711.2002.05377.x.

Cunha MS, Alentiev D, Brandão IM and Perraut K (2013), Dec. Testing excitation models of rapidly oscillating Ap stars with interferometry. *MNRAS* 436: 1639–1647. doi:10.1093/mnras/stt1679. 1310.3019.

Daszyńska-Daszkiewicz J, Pamyatnykh AA, Walczak P, Handler G, Pigulski A and Szewczuk W (2021), Jul. Mode identification and seismic study of δ Scuti, the prototype of a class of pulsating stars. *MNRAS* 505 (1): 88–102. doi:10.1093/mnras/stab1292. 2105.00905.

Dupret MA, Thoul A, Scuflaire R, Daszyńska-Daszkiewicz J, Aerts C, Bourge PO, Waelkens C and Noels A (2004), Feb. Asteroseismology of the β Cep star HD 129929. II. Seismic constraints on core overshooting, internal rotation and stellar parameters. *A&A* 415: 251–257. doi:10.1051/0004-6361:20034143.

Dziembowski WA and Goode PR (1992), Aug. Effects of differential rotation on stellar oscillations - A second-order theory. *ApJ* 394: 670–687. doi:10.1086/171621.

Dziembowski WA and Pamyatnykh AA (1993), May. The opacity mechanism in B-type stars. I - Unstable modes in Beta Cephei star models. *MNRAS* 262: 204–212.

Dziembowski WA, Moskalik P and Pamyatnykh AA (1993), Dec. The Opacity Mechanism in B-Type Stars - Part Two - Excitation of High-Order G-Modes in Main Sequence Stars. *MNRAS* 265: 588.

Fontaine G and Brassard P (2008), Oct. The Pulsating White Dwarf Stars. 120: 1043–1096. doi:10.1086/592788.

Fuller J, Cantiello M, Stello D, Garcia RA and Bildsten L (2015), Oct. Asteroseismology can reveal strong internal magnetic fields in red giant stars. *Science* 350 (6259): 423–426. doi:10.1126/science.aac6933. 1510.06960.

Gaia Collaboration, Prusti T, de Bruijne JHJ, Brown AGA, Vallenari A, Babusiaux C, Bailer-Jones CAL, Bastian U, Biermann M, Evans DW, Eyer

L, Jansen F, Jordi C, Klioner SA, Lammers U, Lindegren L, Luri X, Mignard F, Milligan DJ, Panem C, Poinsignon V, Pourbaix D, Randich S, Sarri G, Sartoretti P, Siddiqui HI, Soubiran C, Valette V, van Leeuwen F, Walton NA, Aerts C, Arenou F, Cropper M, Drimmel R, Høg E, Katz D, Lattanzi MG, O'Mullane W, Grebel EK, Holland AD, Huc C, Passot X, Bramante L, Cacciari C, Castañeda J, Chaoul L, Cheek N, De Angeli F, Fabricius C, Guerra R, Hernández J, Jean-Antoine-Piccolo A, Masana E, Messineo R, Mowlavi N, Nienartowicz K, Ordóñez-Blanco D, Panuzzo P, Portell J, Richards PJ, Riello M, Seabroke GM, Tanga P, Thévenin F, Torra J, Els SG, Gracia-Abril G, Comoretto G, Garcia-Reinaldos M, Lock T, Mercier E, Altmann M, Andrae R, Astraatmadja TL, Bellas-Velidis I, Benson K, Berthier J, Blomme R, Busso G, Carry B, Cellino A, Clementini G, Cowell S, Creevey O, Cuypers J, Davidson M, De Ridder J, de Torres A, Delchambre L, Dell'Oro A, Ducourant C, Frémat Y, García-Torres M, Gosset E, Halbwachs JL, Hambly NC, Harrison DL, Hauser M, Hestroffer D, Hodgkin ST, Huckle HE, Hutton A, Jasniewicz G, Jordan S, Kontizas M, Korn AJ, Lanzafame AC, Manteiga M, Moitinho A, Muinonen K, Osinde J, Pancino E, Pauwels T, Petit JM, Recio-Blanco A, Robin AC, Sarro LM, Siopis C, Smith M, Smith KW, Sozzetti A, Thuillot W, van Reeven W, Viala Y, Abbas U, Abreu Aramburu A, Accart S, Aguado JJ, Allan PM, Allasia W, Altavilla G, Álvarez MA, Alves J, Anderson RI, Andrei AH, Anglada Varela E, Antiche E, Antoja T, Antón S, Arcay B, Atzei A, Ayache L, Bach N, Baker SG, Balaguer-Núñez L, Barache C, Barata C, Barbier A, Barblan F, Baroni M, Barrado y Navascués D, Barros M, Barstow MA, Becciani U, Bellazzini M, Bellei G, Bello García A, Belokurov V, Bendjoya P, Berihuete A, Bianchi L, Bienaymé O, Billebaud F, Blagorodnova N, Blanco-Cuaresma S, Boch T, Bombrun A, Borrachero R, Bouquillon S, Bourda G, Bouy H, Bragaglia A, Breddels MA, Brouillet N, Brüsemeister T, Bucciarelli B, Budnik F, Burgess P, Burgon R, Burlacu A, Busonero D, Buzzi R, Caffau E, Cambras J, Campbell H, Cancelliere R, Cantat-Gaudin T, Carlucci T, Carrasco JM, Castellani M, Charlot P, Charnas J, Charvet P, Chassat F, Chiavassa A, Clotet M, Cocozza G, Collins RS, Collins P, Costigan G, Crifo F, Cross NJG, Crosta M, Crowley C, Dafonte C, Damerdji Y, Dapergolas A, David P, David M, De Cat P, de Felice F, de Laverny P, De Luise F, De March R, de Martino D, de Souza R, Debosscher J, del Pozo E, Delbo M, Delgado A, Delgado HE, di Marco F, Di Matteo P, Diakite S, Distefano E, Dolding C, Dos Anjos S, Drazinos P, Durán J, Dzigan Y, Ecale E, Edvardsson B, Enke H, Erdmann M, Escolar D, Espina M, Evans NW, Eynard Bontemps G, Fabre C, Fabrizio M, Faigler S, Falcão AJ, Farràs Casas M, Faye F, Federici L, Fedorets G, Fernández-Hernández J, Fernique P, Fienga A, Figueras F, Filippi F, Findeisen K, Fonti A, Fouesneau M, Fraile E, Fraser M, Fuchs J, Furnell R, Gai M, Galleti S, Galluccio L, Garabato D, García-Sedano F, Garé P, Garofalo A, Garralda N, Gavras P, Gerssen J, Geyer R, Gilmore G, Girona S, Giuffrida G, Gomes M, González-Marcos A, González-Núñez J, González-Vidal JJ, Granvik M, Guerrier A, Guillout P, Guiraud J, Gúrpide A, Gutiérrez-Sánchez R, Guy LP, Haigron R, Hatzidimitriou D, Haywood M, Heiter U, Helmi A, Hobbs D, Hofmann W, Holl B, Holland G, Hunt JAS, Hypki A, Icardi V, Irwin M, Jevardat de Fombelle G, Jofré P, Jonker PG, Jorissen A, Julbe F, Karampelas A, Kochoska A, Kohley R, Kolenberg K, Kontizas E, Koposov SE, Kordopatis G, Koubsky P, Kowalczyk A, Krone-Martins A, Kudryashova M, Kull I, Bachchan RK, Lacoste-Seris F, Lanza AF, Lavigne JB, Le Poncin-Lafitte C, Lebreton Y, Lebzelter T, Leccia S, Leclerc N, Lecoeur-Taibi I, Lemaitre V, Lenhardt H, Leroux F, Liao S, Licata E, Lindstrøm HEP, Lister TA, Livanou E, Lobel A, Löffler W, López M, Lopez-Lozano A, Lorenz D, Loureiro T, MacDonald I, Magalhães Fernandes T, Managau S, Mann RG, Mantelet G, Marchal O, Marchant JM, Marconi M, Marie J, Marinoni S, Marrese PM, Marschalkó G, Marshall DJ, Martín-Fleitas JM, Martino M, Mary N, Matijevič G, Mazeh T, McMillan PJ, Messina S, Mestre A, Michalik D, Millar NR, Miranda BMH, Molina D, Molinaro R, Molinaro M, Molnár L, Moniez M, Montegriffo P, Monteiro D, Mor R, Mora A, Morbidelli R, Morel T, Morgenthaler S, Morley T, Morris D, Mulone AF, Muraveva T, Musella I, Narbonne J, Nelemans G, Nicastro L, Noval L, Ordénovic C, Ordieres-Meré J, Osborne P, Pagani C, Pagano I, Pailler F, Palacin H, Palaversa L, Parsons P, Paulsen T, Pecoraro M, Pedrosa R, Pentikäinen H, Pereira J, Pichon B, Piersimoni AM, Pineau FX, Plachy E, Plum G, Poujoulet E, Prša A, Pulone L, Ragaini S, Rago S, Rambaux N, Ramos-Lerate M, Ranalli P, Rauw G, Read A, Regibo S, Renk F, Reylé C, Ribeiro RA, Rimoldini L, Ripepi V, Riva A, Rixon G, Roelens M, Romero-Gómez M, Rowell N, Royer F, Rudolph A, Ruiz-Dern L, Sadowski G, Sagristà Sellés T, Sahlmann J, Salgado J, Salguero E, Sarasso M, Savietto H, Schnorhk A, Schultheis M, Sciacca E, Segol M, Segovia JC, Segransan D, Serpell E, Shih IC, Smareglia R, Smart RL, Smith C, Solano E, Solitro F, Sordo R, Soria Nieto S, Souchay J, Spagna A, Spoto F, Stampa U, Steele IA, Steidelmüller H, Stephenson CA, Stoev H, Suess FF, Süveges M, Surdej J, Szabados L, Szegedi-Elek E, Tapiador D, Taris F, Tauran G, Taylor MB, Teixeira R, Terrett D, Tingley B, Trager SC, Turon C, Ulla A, Utrilla E, Valentini G, van Elteren A, Van Hemelryck E, van Leeuwen M, Varadi M, Vecchiato A, Veljanoski J, Via T, Vicente D, Vogt S, Voss H, Votruba V, Voutsinas S, Walmsley G, Weiler M, Weingrill K, Werner D, Wevers T, Whitehead G, Wyrzykowski Ł, Yoldas A, Žerjal M, Zucker S, Zurbach C, Zwitter T, Alecu A, Allen M, Allende Prieto C, Amorim A, Anglada-Escudé G, Arsenijevic V, Azaz S, Balm P, Beck M, Bernstein HH, Bigot L, Bijaoui A, Blasco C, Bonfigli M, Bono G, Boudreault S, Bressan A, Brown S, Brunet PM, Bunclark P, Buonanno R, Butkevich AG, Carret C, Carrion C, Chemin L, Chéreau F, Corcione L, Darmigny E, de Boer KS, de Teodoro P, de Zeeuw PT, Delle Luche C, Domingues CD, Dubath P, Fodor F, Frézouls B, Fries A, Fustes D, Fyfe D, Gallardo E, Gallegos J, Gardiol D, Gebran M, Gomboc A, Gómez A, Grux E, Gueguen A, Heyrovsky A, Hoar J, Iannicola G, Isasi Parache Y, Janotto AM, Joliet E, Jonckheere A, Keil R, Kim DW, Klagyivik P, Klar J, Knude J, Kochukhov O, Kolka I, Kos J, Kutka A, Lainey V, LeBouquin D, Liu C, Loreggia D, Makarov VV, Marseille MG, Martayan C, Martinez-Rubi O, Massart B, Meynadier F, Mignot S, Munari U, Nguyen AT, Nordlander T, Ocvirk P, O'Flaherty KS, Olias Sanz A, Ortiz P, Osorio J, Oszkiewicz D, Ouzounis A, Palmer M, Park P, Pasquato E, Peltzer C, Peralta J, Péturaud F, Pieniluoma T, Pigozzi E, Poels J, Prat G, Prod'homme T, Raison F, Rebordao JM, Risquez D, Rocca-Volmerange B, Rosen S, Ruiz-Fuertes MI, Russo F, Sembay S, Serraller Vizcaino I, Short A, Siebert A, Silva H, Sinachopoulos D, Slezak E, Soffel M, Sosnowska D, Straižys V, ter Linden M, Terrell D, Theil S, Tiede C, Troisi L, Tsalmantza P, Tur D, Vaccari M, Vachier F, Valles P, Van Hamme W, Veltz L, Virtanen J, Wallut JM, Wichmann R, Wilkinson MI, Ziaeepour H and Zschocke S (2016), Nov. The Gaia mission. *A&A* 595, A1. doi:10.1051/0004-6361/201629272. 1609.04153.

Gehan C, Mosser B, Michel E, Samadi R and Kallinger T (2018), Aug. Core rotation braking on the red giant branch for various mass ranges. *A&A* 616, A24. doi:10.1051/0004-6361/201832822. 1802.04558.

Giammichele N, Charpinet S, Fontaine G, Brassard P, Green EM, Van Grootel V, Bergeron P, Zong W and Dupret MA (2018), Feb. A large oxygen-dominated core from the seismic cartography of a pulsating white dwarf. *Nature* 554 (7690): 73–76. doi:10.1038/nature25136.

Glatzel W, Kiriakidis M, Chernigovskij S and Fricke KJ (1999), Feb. The non-linear evolution of strange-mode instabilities. *MNRAS* 303 (1): 116–124. doi:10.1046/j.1365-8711.1999.02190.x.

Guzik JA, Kaye AB, Bradley PA, Cox AN and Neuforge C (2000), Oct. Driving the Gravity-Mode Pulsations in γ Doradus Variables. 542: L57–L60. doi:10.1086/312908.

Hasan SS, Zahn JP and Christensen-Dalsgaard J (2005), Dec. Probing the internal magnetic field of slowly pulsating B-stars through g modes. *A&A* 444 (2): L29–L32. doi:10.1051/0004-6361:200500203. astro-ph/0511472.

Hekker S (2020), Feb. Scaling relations for solar-like oscillations: a review. *Frontiers in Astronomy and Space Sciences* 7, 3. doi:10.3389/fspas.2020.00003. 1907.10457.

Hermes JJ, Gänsicke BT, Kawaler SD, Greiss S, Tremblay PE, Gentile Fusillo NP, Raddi R, Fanale SM, Bell KJ, Dennihy E, Fuchs JT, Dunlap BH, Clemens JC, Montgomery MH, Winget DE, Chote P, Marsh TR and Redfield S (2017), Oct. White Dwarf Rotation as a Function of Mass and a Dichotomy of Mode Line Widths: Kepler Observations of 27 Pulsating DA White Dwarfs through K2 Campaign 8. 232, 23. doi:10.3847/1538-4365/aa8bb5. 1709.07004.

Holdsworth DL, Cunha MS, Lares-Martiz M, Kurtz DW, Antoci V, Barceló Forteza S, De Cat P, Derekas A, Kayhan C, Ozuyar D, Skarka M, Hey DR, Shi F, Bowman DM, Kobzar O, Ayala Gómez A, Bognár Z, Buzasi DL, Ebadi M, Fox-Machado L, García Hernández A, Ghasemi H, Guzik JA, Handberg R, Handler G, Hasanzadeh A, Jayaraman R, Khalack V, Kochukhov O, Lovekin CC, Mikołajczyk P, Mkrtichian D, Murphy SJ,

Niemczura E, Olafsson BG, Pascual-Granado J, Paunzen E, Posiłek N, Ramón-Ballesta A, Safari H, Samadi-Ghadim A, Smalley B, Sódor Á, Stateva I, Suárez JC, Szabó R, Wu T, Ziaali E, Zong W and Seager S (2024), Feb. TESS Cycle 2 observations of roAp stars with 2-min cadence data. *MNRAS* 527 (4): 9548–9580. doi:10.1093/mnras/stad3800. 2312.04199.

Huat AL, Hubert AM, Baudin F, Floquet M, Neiner C, Frémat Y, Gutiérrez-Soto J, Andrade L, de Batz B, Diago PD, Emilio M, Espinosa Lara F, Fabregat J, Janot-Pacheco E, Leroy B, Martayan C, Semaan T, Suso J, Auvergne M, Catala C, Michel E and Samadi R (2009), Oct. The B0.5IVe CoRoT target HD 49330. I. Photometric analysis from CoRoT data. *A&A* 506 (1): 95–101. doi:10.1051/0004-6361/200911928.

Kilkenny D (2007), Jun. Pulsating Hot Subdwarfs – An Observational Review. *Communications in Asteroseismology* 150: 234. doi:10.1553/cia150s234.

Kilkenny D, Koen C, O'Donoghue D and Stobie RS (1997), Mar. A new class of rapidly pulsating star - I. EC 14026-2647, the class prototype. *MNRAS* 285: 640–644. doi:10.1093/mnras/285.3.640.

Kippenhahn R, Weigert A and Weiss A (2012). Stellar Structure and Evolution, Springer. doi:10.1007/978-3-642-30304-3.

Kurtz DW (1982), Sep. Rapidly oscillating AP stars. *MNRAS* 200: 807–859.

Kurtz DW (1985), Apr. An algorithm for significantly reducing the time necessary to compute a Discrete Fourier Transform periodogram of unequally spaced data. *MNRAS* 213: 773–776.

Kurtz DW (1990). Rapidly oscillating AP stars. *Ann. Rev. Astron. Astrophys.* 28: 607–655. doi:10.1146/annurev.aa.28.090190.003135.

Kurtz DW (2022), Aug. Asteroseismology Across the Hertzsprung-Russell Diagram. *Ann. Rev. Astron. Astrophys.* 60: 31–71. doi:10.1146/annurev-astro-052920-094232.

Kurtz DW, Saio H, Takata M, Shibahashi H, Murphy SJ and Sekii T (2014), Oct. Asteroseismic measurement of surface-to-core rotation in a main-sequence A star, KIC 11145123. *MNRAS* 444: 102–116. doi:10.1093/mnras/stu1329. 1405.0155.

Labadie-Bartz J, Carciofi AC, Henrique de Amorim T, Rubio A, Luiz Figueiredo A, Ticiani dos Santos P and Thomson-Paressant K (2022), May. Classifying Be Star Variability With TESS. I. The Southern Ecliptic. *AJ* 163 (5), 226. doi:10.3847/1538-3881/ac5abd.

Langer N (2012), Sep. Presupernova Evolution of Massive Single and Binary Stars. *Ann. Rev. Astron. Astrophys.* 50: 107–164. doi:10.1146/annurev-astro-081811-125534. 1206.5443.

Lecoanet D, Bowman DM and Van Reeth T (2022), May. Asteroseismic inference of the near-core magnetic field strength in the main-sequence B star HD 43317. *MNRAS* 512 (1): L16–L20. doi:10.1093/mnrasl/slac013. 2202.03440.

Li G, Van Reeth T, Bedding TR, Murphy SJ, Antoci V, Ouazzani RM and Barbara NH (2020), Jan. Gravity-mode period spacings and near-core rotation rates of 611 γ Doradus stars with Kepler. *MNRAS* 491 (3): 3586–3605. doi:10.1093/mnras/stz2906. 1910.06634.

Li G, Deheuvels S, Ballot J and Lignières F (2022), Oct. Magnetic fields of 30 to 100 kG in the cores of red giant stars. *Nature* 610 (7930): 43–46. doi:10.1038/s41586-022-05176-0. 2208.09487.

Loi ST (2020), Aug. Effect of a strong magnetic field on gravity-mode period spacings in red giant stars. *MNRAS* 496 (3): 3829–3840. doi:10.1093/mnras/staa1823. 2006.08635.

Mombarg JSG, Van Reeth T, Pedersen MG, Molenberghs G, Bowman DM, Johnston C, Tkachenko A and Aerts C (2019), May. Asteroseismic masses, ages, and core properties of γ Doradus stars using gravito-inertial dipole modes and spectroscopy. *MNRAS* 485 (3): 3248–3263. doi:10.1093/mnras/stz501. 1902.06746.

Mombarg JSG, Van Reeth T and Aerts C (2021), Jun. Constraining stellar evolution theory with asteroseismology of γ Doradus stars using deep learning. Stellar masses, ages, and core-boundary mixing. *A&A* 650, A58. doi:10.1051/0004-6361/202039543.

Moskalik P and Buchler JR (1990), Jun. Resonances and period doubling in the pulsations of stellar models. *ApJ* 355: 590–601. doi:10.1086/168792.

Neiner C, Lee U, Mathis S, Saio H, Lovekin CC and Augustson KC (2020), Dec. Transport of angular momentum by stochastically excited waves as an explanation for the outburst of the rapidly rotating Be star HD49330. *A&A* 644, A9. doi:10.1051/0004-6361/201935858. 2007.08977.

Ouazzani RM, Marques JP, Goupil MJ, Christophe S, Antoci V, Salmon SJAJ and Ballot J (2019), Jun. γ Doradus stars as a test of angular momentum transport models. *A&A* 626, A121. doi:10.1051/0004-6361/201832607. 1801.09228.

Pamyatnykh AA (1999), Jun. Pulsational Instability Domains in the Upper Main Sequence. *Acta Astronomica* 49: 119–148.

Panda SK, Dhanpal S, Murphy SJ, Hanasoge S and Bedding TR (2024), Jan. Asteroseismology Applied to Constrain Structure Parameters of δ Scuti Stars. *ApJ* 960 (2), 94. doi:10.3847/1538-4357/ad0a97. 2310.07203.

Pápics PI, Tkachenko A, Van Reeth T, Aerts C, Moravveji E, Van de Sande M, De Smedt K, Bloemen S, Southworth J, Debosscher J, Niemczura E and Gameiro JF (2017), Feb. Signatures of internal rotation discovered in the Kepler data of five slowly pulsating B stars. *A&A* 598, A74. doi:10.1051/0004-6361/201629814. 1611.06955.

Pedersen MG, Aerts C, Pápics PI, Michielsen M, Gebruers S, Rogers TM, Molenberghs G, Burssens S, Garcia S and Bowman DM (2021), Jan. Internal mixing of rotating stars inferred from dipole gravity modes. *Nature Astronomy* 5: 715–722. doi:10.1038/s41550-021-01351-x. 2105.04533.

Petersen JO (1973), Aug. Masses of double mode cepheid variables determined by analysis of period ratios. *A&A* 27: 89–93.

Rauer H, Aerts C, Cabrera J, Deleuil M, Erikson A, Gizon L, Goupil M, Heras A, Lorenzo-Alvarez J, Marliani F, Martin-Garcia C, Mas-Hesse JM, O'Rourke L, Osborn H, Pagano I, Piotto G, Pollacco D, Ragazzoni R, Ramsay G, Udry S, Appourchaux T, Benz W, Brandeker A, Güdel M, Janot-Pacheco E, Kabath P, Kjeldsen H, Min M, Santos N, Smith A, Suarez JC, Werner SC, Aboudan A, Abreu M, Acuña L, Adams M, Adibekyan V, Affer L, Agneray F, Agnor C, Aguirre Børsen-Koch V, Ahmed S, Aigrain S, Al-Bahlawan A, Alcacera Gil MdlA, Alei E, Alencar S, Alexander R, Alfonso-Garzón J, Alibert Y, Allende Prieto C, Almeida L, Alonso Sobrino R, Altavilla G, Althaus C, Alonso Alvarez Trujillo L, Amarsi A, Ammler-von Eiff M, Amôres E, Andrade L, Antoniadis-Karnavas A, António C, Aparicio del Moral B, Appolloni M, Arena C, Armstrong D, Aroca Aliaga J, Asplund M, Audenaert J, Auricchio N, Avelino P, Baeke A, Baillié K, Balado A, Balestra A, Ball W, Ballans H, Ballot J, Barban C, Barbary G, Barbieri M, Barceló Forteza S, Barker A, Barklem P, Barnes S, Barrado Navascues D, Barragan O, Baruteau C, Basu S, Baudin F, Baumeister P, Bayliss D, Bazot M, Beck PG, Bedding T, Belkacem K, Bellinger E, Benatti S, Benomar O, Bérard D, Bergemann M, Bergomi M, Bernardo P, Biazzo K, Bignamini A, Bigot L, Billot N, Binet M, Biondi D, Biondi F, Birch AC, Bitsch B, Bluhm Ceballos PV, Bódi A, Bognár Z, Boisse I, Bolmont E, Bonanno A, Bonavita M, Bonfanti A, Bonfils X, Bonito R, Bonomo AS, Börner A, Boro Saikia S, Borreguero Martín E, Borsa F, Borsato L, Bossini D, Bouchy F, Boué G, Boufleur R, Boumier P, Bourrier V, Bowman DM, Bozzo E, Bradley L, Bray J, Bressan A, Breton S, Brienza D, Brito A, Brogi M, Brown B, Brown D, Brun AS, Bruno G, Bruns M, Buchhave LA, Bugnet L, Buldgen G, Burgess P, Busatta A, Busso G, Buzasi D, Caballero JA, Cabral A, Calderone F, Cameron R, Cameron A, Campante T, Canto Martins BL, Cara C, Carone L, Carrasco JM, Casagrande L, Casewell SL, Cassisi S, Castellani M, Castro M, Catala C, Catalán Fernández I, Catelan M, Cegla H, Cerruti C, Cessa V, Chadid M, Chaplin W, Charpinet S, Chiappini C, Chiarucci S, Chiavassa A, Chinellato S, Chirulli G, Christensen-Dalsgaard J, Church R, Claret A, Clarke C, Claudi R, Clermont L, Coelho H, Coelho J, Cogato F, Colomé J, Condamin M, Conseil S, Corbard T, Correia ACM, Corsaro E, Cosentino R, Costes J, Cottinelli A, Covone G, Creevey OL, Crida A, Csizmadia S, Cunha M, Curry P, da Costa J, da Silva F, Dalal S, Damasso M, Damiani C, Damiani F, Liduina das Chagas M, Davies M, Davies G, Davies B, Davison G, de Almeida L, de Angeli F, Cabral de Barros SC, de Castro Leão I, Brito de Freitas D, de Freitas MC, De Martino D, Renan de Medeiros J, de Paula LA, de Plaa J, De Ridder J, Deal M, Decin L, Deeg H, Degl'Innocenti S, Deheuvels S, del Burgo C, Del Sordo F, Delgado-Mena

E, Demangeon O, Denk T, Derekas A, Desidera S, Dexet M, Di Criscienzo M, Di Giorgio AM, Di Mauro MP, Diaz Rial FJ, Díaz-García JJ, Dima M, Dinuzzi G, Dionatos O, Distefano E, do Nascimento Jose-Dias J, Domingo A, D'Orazi V, Dorn C, Doyle L, Duarte E, Ducellier F, Dumaye L, Dumusque X, Dupret MA, Eggenberger P, Ehrenreich D, Eigmüller P, Eising J, Emilio M, Eriksson K, Ermocida M, Isidoro Escate Giribaldi R, Eschen Y, Estrela I, Evans DW, Fabbian D, Fabrizio M, Faria JP, Farina M, Farinato J, Feliz D, Feltzing S, Fenouillet T, Ferrari L, Ferraz-Mello S, Fialho F, Fienga A, Figueira P, Fiori L, Flaccomio E, Focardi M, Foley S, Fontignie J, Ford D, Fornazier K, Forveille T, Fossati L, de Marca Franca R, da Silva LF, Frasca A, Fridlund M, Furlan M, Gabler SM, Gaido M, Gallagher A, Galli E, Garcia RA, García Hernández A, Garcia Munoz A, García-Vázquez H, Garrido Haba R, Gaulme P, Gauthier N, Gehan C, Gent M, Georgieva I, Ghigo M, Giana E, Gill S, Girardi L, Giuliatti Winter S, Giusi G, Gomes da Silva J, Gómez Zazo LJ, Gomez-Lopez JM, Isai González Hernández J, Gonzalez Murillo K, Gorius N, Gouel PV, Goulty D, Granata V, Grenfell JL, Grießbach D, Grolleau E, Grouffal S, Grziwa S, Guarcello MG, Gueguen L, Guenther EW, Guilhem T, Guillerot L, Guiot P, Guterman P, Gutiérrez A, Gutiérrez-Canales F, Hagelberg J, Haldemann J, Hall C, Handberg R, Harrison I, Harrison DL, Hasiba J, Haswell CA, Hatalova P, Hatzes A, Haywood R, Hébrard G, Heckes F, Heiter U, Hekker S, Heller R, Helling C, Helminiak K, Hemsley S, Heng K, Hermans A, Hermes J, Hidalgo Torres N, Hinkel N, Hobbs D, Hodgkin S, Hofmann K, Hojjatpanah S, Houdek G, Huber D, Huesler J, Hui-Bon-Hoa A, Huygen R, Huynh DD, Iro N, Irwin J, Irwin M, Izidoro A, Jacquinod S, Emborg Jannsen N, Janson M, Jeszenszky H, Jiang C, José Jimenez Mancebo A, Jofre P, Johansen A, Johnston C, Jones G, Kallinger T, Kálmán S, Kanitz T, Karjalainen M, Karjalainen R, Karoff C, Kawaler S, Kawata D, Keereman A, Keiderling D, Kennedy T, Kenworthy M, Kerschbaum F, Kidger M, Kiefer F, Kintziger C, Kislyakova K, Kiss L, Klagyivik P, Klahr H, Klevas J, Kochukhov O, Köhler U, Kolb U, Koncz A, Korth J, Kostogryz N, Kovács G, Kovács J, Kozhura O, Krivova N, Kučinskas A, Kuhlemann I, Kupka F, Laauwen W, Labiano A, Lagarde N, Laget P, Laky G, Lam KWF, Lambrechts M, Lammer H, Lanza AF, Lanzafame A, Lares Martiz M, Laskar J, Latter H, Lavanant T, Lawrenson A, Lazzoni C, Lebre A, Lebreton Y, Lecavelier des Etangs A, Leinhardt Z, Leleu A, Lendl M, Leto G, Levillain Y, Libert AS, Lichtenberg T, Ligi R, Lignieres F, Lillo-Box J, Linsky J, Scige Liu J, Loidolt D, Longval Y, Lopes I, Lorenzani A, Ludwig HG, Lund M, Sloth Lundkvist M, Luri X, Maceroni C, Madden S, Madhusudhan N, Maggio A, Magliano C, Magrin D, Mahy L, Maibaum O, Malac-Allain L, Malapert JC, Malavolta L, Maldonado J, Mamonova E, Manchon L, Mann A, Mantovan G, Marafatto L, Marconi M, Mardling R, Marigo P, Marinoni S, Marques É, Marques JP, Marrese PM, Marshall D, Martínez Perales S, Mary D, Marzari F, Masana E, Mascher A, Mathis S, Mathur S, Mattiuci Figueiredo AC, Maxted PFL, Mazeh T, Mazevet S, Mazzei F, McCormac J, McMillan P, Menou L, Merle T, Meru F, Mesa D, Messina S, Mészáros S, Meunier N, Meunier JC, Micela G, Michaelis H, Michel E, Michielsen M, Michtchenko T, Miglio A, Miguel Y, Milligan D, Mirouh G, Mitchel M, Moedas N, Molendini F, Molnár L, Mombarg J, Montalban J, Montalto M, Monteiro MJPFG, Morales JC, Morales-Calderon M, Morbidelli A, Mordasini C, Moreau C, Morel T, Morello G, Morin J, Mortier A, Mosser B, Mourard D, Mousis O, Moutou C, Mowlavi N, Moya A, Muehlmann P, Muirhead P, Munari M, Musella I, Mustill AJ, Nardetto N, Nardiello D, Narita N, Nascimbeni V, Nash A, Neiner C, Nelson RP, Nettelmann N, Nicolini G, Nielsen M, Niemi SM, Noack L, Noels-Grotsch A, Noll A, Norazman A, Norton AJ, Nsamba B, Ofir A, Ogilvie G, Olander T, Olivetto C, Olofsson G, Ong J, Ortolani S, Oshagh M, Ottacher H, Ottensamer R, Ouazzani RM, Paardekooper SJ, Pace E, Pajas M, Palacios A, Palandri G, Palle E, Paproth C, Parro V, Parviainen H, Granado JP, Passegger VM, Pastor-Morales C, Pätzold M, Gade Pedersen M, Pena Hidalgo D, Pepe F, Pereira F, Persson CM, Pertenais M, Peter G, Petit AC, Petit P, Pezzuto S, Pichierri G, Pietrinferni A, Pinheiro F, Pinsonneault M, Plachy E, Plasson P, Plez B, Poppenhaeger K, Poretti E, Portaluri E, Portell J, Frederico Porto de Mello G, Poyatos J, Pozuelos FJ, Prada Moroni PG, Pricopi D, Prisinzano L, Quade M, Quirrenbach160 n, Rabanal Reina6 JA, Rabello Soares MC, Raimondo G, Rainer M, Ramón Rodón J, Ramón-Ballesta A, Ramos Zapata G, Rätz S, Rauterberg C, Redman B, Redmer R, Reese D, Regibo S, Reiners A, Reinhold T, Renie C, Ribas I, Ribeiro S, Pereira Ricciardi T, Rice K, Richard O, Riello M, Rieutord M, Ripepi V, Rixon G, Rockstein S, Rodríguez MTR, Rodríguez Díaz LF, Rodriguez Garcia JP, Rodriguez-Gomez J, Roehlly Y, Roig F, Rojas-Ayala B, Rolf T, Lysgaard Rørsted J, Rosado H, Rosotti G, Roth O, Roth M, Rousseau A, Roxburgh I, Roy F, Royer P, Ruane K, Rufini Mastropasqua S, Ruiz de Galarreta C, Russi A, Saar S, Saillenfest M, Salaris M, Salmon S, Saltas I, Samadi R, Samadi A, Samra D, Sanches da Silva T, Andrés Sánchez Carrasco M, Santerne A, Santoli F, Santos ÂRG, Sanz Mesa R, Sarro LM, Scandariato G, Schäfer M, Schlafly E, Schmider FX, Schneider J, Schou J, Schunker H, Jörg Schwarzkopf G, Serenelli A, Seynaeve D, Shan Y, Shapiro A, Shipman R, Sicilia D, Sierra Sanmartin MA, Sigot A, Silliman K, Silvotti R, Simon AE, Simoyama Napoli R, Skarka M, Smalley B, Smiljanic R, Smit S, Smith A, Smith L, Snellen I, Sódor Á, Sohl F, Solanki SK, Sortino F, Sousa S, Southworth J, Souto D, Sozzetti A, Stamatellos D, Stassun K, Steller M, Stello D, Stelzer B, Stiebeler U, Stokholm A, Storelvmo T, Strassmeier K, Strøm PA, Strugarek A, Sulis S, Švanda M, Szabados L, Szabó R, Szabó GM, Szuszkiewicz E, Talens GJ, Teti D, Theisen T, Thévenin F, Thoul A, Tiphene D, Titz-Weider R, Tkachenko A, Tomecki D, Tonfat J, Tosi N, Trampedach R, Traven G, Triaud A, Trønnes R, Tsantaki M, Tschentscher M, Turin A, Tvaruzka A, Ulmer B, Ulmer-Moll S, Ulusoy C, Umbriaco G, Valencia D, Valentini M, Valio A, Valverde Guijarro ÁL, Van Eylen V, Van Grootel V, van Kempen TA, Van Reeth T, Van Zelst I, Vandenbussche B, Vasiliou K, Vasilyev V, Vaz de Mascarenhas D, Vazan A, Vela Nunez M, Nunes Velloso E, Ventura R, Ventura P, Venturini J, Trallero IV, Veras D, Verdugo E, Verma K, Vibert D, Vicanek Martinez T, Vida K, Vigan A, Villacorta A, Villaver E, Villaverde Aparicio M, Viotto V, Vorobyov E, Vorontsov S, Wagner FW, Walloschek T, Walton N, Walton D, Wang H, Waters R, Watson C, Wedemeyer S, Weeks A, Weingril J, Weiss A, Wendler B, West R, Westerdorff K, Westphal PA, Wheatley P, White T, Whittaker A, Wickhusen K, Wilson T, Windsor J, Winter O, Lykke Winther M, Winton A, Witteck U, Witzke V, Woitke P, Wolter D, Wuchterl G, Wyatt M, Yang D, Yu J, Zanmar Sanchez R, Rosa Zapatero Osorio M, Zechmeister M, Zhou Y, Ziemke C and Zwintz K (2024), Jun. The PLATO Mission. *arXiv e-prints* , arXiv:2406.05447doi:10.48550/arXiv.2406.05447. 2406.05447.

Ricker GR, Winn JN, Vanderspek R, Latham DW, Bakos GÁ, Bean JL, Berta-Thompson ZK, Brown TM, Buchhave L, Butler NR, Butler RP, Chaplin WJ, Charbonneau D, Christensen-Dalsgaard J, Clampin M, Deming D, Doty J, De Lee N, Dressing C, Dunham EW, Endl M, Fressin F, Ge J, Henning T, Holman MJ, Howard AW, Ida S, Jenkins JM, Jernigan G, Johnson JA, Kaltenegger L, Kawai N, Kjeldsen H, Laughlin G, Levine AM, Lin D, Lissauer JJ, MacQueen P, Marcy G, McCullough PR, Morton TD, Narita N, Paegert M, Palle E, Pepe F, Pepper J, Quirrenbach A, Rinehart SA, Sasselov D, Sato B, Seager S, Sozzetti A, Stassun KG, Sullivan P, Szentgyorgyi A, Torres G, Udry S and Villasenor J (2015), Jan. Transiting Exoplanet Survey Satellite (TESS). *Journal of Astronomical Telescopes, Instruments, and Systems* 1 (1), 014003. doi:10.1117/1.JATIS.1.1.014003.

Rivinius T, Carciofi AC and Martayan C (2013), Oct. Classical Be stars. Rapidly rotating B stars with viscous Keplerian decretion disks. 21, 69. doi:10.1007/s00159-013-0069-0. 1310.3962.

Scargle JD (1982), Dec. Studies in astronomical time series analysis. II. Statistical aspects of spectral analysis of unevenly spaced data. *ApJ* 263: 835–853. doi:10.1086/160554.

Stellingwerf RF (1975), Jan. Modal stability of RR Lyrae stars. *ApJ* 195: 441–466. doi:10.1086/153343.

Stello D, Cantiello M, Fuller J, Huber D, García RA, Bedding TR, Bildsten L and Silva Aguirre V (2016), Jan. A prevalence of dynamo-generated magnetic fields in the cores of intermediate-mass stars. *Nature* 529 (7586): 364–367. doi:10.1038/nature16171. 1601.00004.

Suárez JC, Andrade L, Goupil MJ and Janot-Pacheco E (2010), Dec. On the use of rotational splitting asymmetries to probe the internal rotation profile of stars: Application to β Cephei stars. *Astronomische Nachrichten* 331: 1073. doi:10.1002/asna.201011460. 1004.0609.

Szabó R, Benkő JM, Paparó M, Chapellier E, Poretti E, Baglin A, Weiss WW, Kolenberg K, Guggenberger E and Le Borgne JF (2014), Oct. Revisiting CoRoT RR Lyrae stars: detection of period doubling and temporal variation of additional frequencies. *A&A* 570, A100. doi:10.1051/0004-6361/201424522. 1408.0653.

Szewczuk W and Daszyńska-Daszkiewicz J (2017), Jul. Domains of pulsational instability of low-frequency modes in rotating upper main

sequence stars. *MNRAS* 469: 13–46. doi:10.1093/mnras/stx738. 1703.08075.

Szewczuk W, Walczak P and Daszyńska-Daszkiewicz J (2021), Jun. Variability of newly identified B-type stars observed by Kepler. *MNRAS* 503 (4): 5894–5928. doi:10.1093/mnras/stab683. 2103.06146.

Townsend RHD (2005), Dec. Kappa-mechanism excitation of retrograde mixed modes in rotating B-type stars. *MNRAS* 364: 573–582. doi:10.1111/j.1365-2966.2005.09585.x. astro-ph/0506580.

Townsend RHD, Goldstein J and Zweibel EG (2018), Mar. Angular momentum transport by heat-driven g-modes in slowly pulsating B stars. *MNRAS* 475: 879–893. doi:10.1093/mnras/stx3142. 1712.02420.

Uytterhoeven K, Moya A, Grigahcène A, Guzik JA, Gutiérrez-Soto J, Smalley B, Handler G, Balona LA, Niemczura E, Fox Machado L, Benatti S, Chapellier E, Tkachenko A, Szabó R, Suárez JC, Ripepi V, Pascual J, Mathias P, Martín-Ruíz S, Lehmann H, Jackiewicz J, Hekker S, Gruberbauer M, García RA, Dumusque X, Díaz-Fraile D, Bradley P, Antoci V, Roth M, Leroy B, Murphy SJ, De Cat P, Cuypers J, Kjeldsen H, Christensen-Dalsgaard J, Breger M, Pigulski A, Kiss LL, Still M, Thompson SE and van Cleve J (2011), Oct. The Kepler characterization of the variability among A- and F-type stars. I. General overview. *A&A* 534, A125. doi:10.1051/0004-6361/201117368. 1107.0335.

Van Reeth T, Tkachenko A and Aerts C (2016), Oct. Interior rotation of a sample of γ Doradus stars from ensemble modelling of their gravity-mode period spacings. *A&A* 593, A120. doi:10.1051/0004-6361/201628616. 1607.00820.

Vanlaer V, Aerts C, Bellinger EP and Christensen-Dalsgaard J (2023), Jul. Feasibility of structure inversions for gravity-mode pulsators. *A&A* 675, A17. doi:10.1051/0004-6361/202245597. 2305.09624.

Wallerstein G (2002), Jul. The Cepheids of Population II and Related Stars. 114: 689–699. doi:10.1086/341698.

Winget DE and Kepler SO (2008), Sep. Pulsating White Dwarf Stars and Precision Asteroseismology. *Ann. Rev. Astron. Astrophys.* 46: 157–199. doi:10.1146/annurev.astro.46.060407.145250. 0806.2573.

Zong W, Charpinet S and Vauclair G (2016), Oct. Signatures of nonlinear mode interactions in the pulsating hot B subdwarf star KIC 10139564. *A&A* 594, A46. doi:10.1051/0004-6361/201629132. 1607.06621.

Zwintz K, Fossati L, Ryabchikova T, Guenther D, Aerts C, Barnes TG, Themeßl N, Lorenz D, Cameron C, Kuschnig R, Pollack-Drs S, Moravveji E, Baglin A, Matthews JM, Moffat AFJ, Poretti E, Rainer M, Rucinski SM, Sasselov D and Weiss WW (2014), Aug. Echography of young stars reveals their evolution. *Science* 345: 550–553. doi:10.1126/science.1253645. 1407.4928.